

INFLAMMATION

Quantitative analysis of competitive cytokine signaling predicts tissue thresholds for the propagation of macrophage activation

James Bagnall¹, Christopher Boddington¹, Hazel England¹, Ruth Brignall¹, Polly Downton¹, Zainab Alsoufi², James Boyd^{1,3}, William Rowe^{1,4}, Alexander Bennett¹, Catherine Walker¹, Antony Adamson¹, Nisha M. X. Patel¹, Ronan O’Cualain¹, Lorraine Schmidt¹, David G. Spiller¹, Dean A. Jackson¹, Werner Müller¹, Mark Muldoon², Michael R. H. White¹, Pawel Paszek^{1*}

Copyright © 2018
The Authors, some
rights reserved;
exclusive licensee
American Association
for the Advancement
of Science. No claim
to original U.S.
Government Works

Toll-like receptor (TLR) signaling regulates macrophage activation and effector cytokine propagation in the constrained environment of a tissue. In macrophage populations, TLR4 stimulates the dose-dependent transcription of nuclear factor κ B (NF- κ B) target genes. However, using single-RNA counting, we found that individual cells exhibited a wide range (three orders of magnitude) of expression of the gene encoding the proinflammatory cytokine tumor necrosis factor- α (TNF- α). The TLR4-induced *TNFA* transcriptional response correlated with the extent of NF- κ B signaling in the cells and their size. We compared the rates of TNF- α production and uptake in macrophages and mouse embryonic fibroblasts and generated a mathematical model to explore the heterogeneity in the response of macrophages to TLR4 stimulation and the propagation of the TNF- α signal in the tissue. The model predicts that the local propagation of the TLR4-dependent TNF- α response and cellular NF- κ B signaling are limited to small distances of a few cell diameters between neighboring tissue-resident macrophages. In our predictive model, TNF- α propagation was constrained by competitive uptake of TNF- α from the environment, rather than by heterogeneous production of the cytokine. We propose that the highly constrained architecture of tissues enables effective localized propagation of inflammatory cues while avoiding out-of-context responses at longer distances.

INTRODUCTION

Mammals have central cellular defense systems that resist infection by a range of pathogens. These include the Toll-like receptor (TLR) signaling system, members of which decode evolutionarily conserved pathogen-associated molecular patterns into complex transcriptional effector responses (1). Signaling downstream of TLR4 is essential for generating responses to types of lipopolysaccharide (LPS) present on the cell wall of Gram-negative bacteria (2) and involves activation of a large signaling network including the nuclear factor κ B (NF- κ B) and interferon regulatory factor transcription factors (3–5). The regulated gene response involves rapid and temporally coordinated production and secretion of various signaling mediators, including the proinflammatory cytokine tumor necrosis factor- α (TNF- α) (6, 7). Secretion of TNF- α (and potentially other cytokines) activates a cellular cytokine network, which may propagate the antibacterial response in the infected tissue (8). TNF- α acts through its cognate receptors and induces oscillatory responses of the NF- κ B transcription factor in single cells (9–14), which then stimulates the production of TNF- α and other proinflammatory cytokines (15), thereby potentially constituting a positive feedback that enables signal propagation between cells (16, 17). However, unconstrained TNF- α activation is often associated with pathological inflammation, as highlighted by the clinical success of anti-TNF- α therapeutics in arthritis and inflammatory bowel disease (18). The balance between

a rapid immune cell activation and controllable propagation of the response is a fundamental, yet not fully understood, aspect of inflammatory signaling.

Single-cell immune responses are often extremely noisy, as exhibited by NF- κ B dynamics (3–5, 19) and effector cytokine production (20–22). This heterogeneity has been previously linked with population-level robustness (11, 20, 23, 24). However, the earliest stages of the immune response may rely on individual cells rather than on population-level responses (25). One of the first lines of defense against pathogens are resident innate immune cells, which are present within dense matrices a few tens of micrometers apart and are spatially isolated from each other by nonimmune connective tissue (26). This grid-like architecture is conserved in multiple tissues (27), for example, in the retina (28), central nervous system (29), liver (30), and skin (31), and is thought to reflect the capacity of individual immune cells to survey limited numbers of (nonimmune) cells in the tissue (25). The physical separation between immune cells may also provide an additional level of control over noisy paracrine signals in the tissue (32). For example, during the adaptive immune response, effector T cells produce steep cytokine gradients permitting long-range (up to 80 μ m) activation of bystander cells beyond sites of antigen presentation (33). This signaling range may be controlled by secretion kinetics and competitive uptake in dense multicellular environments (34–37).

Ultimately, an understanding of the early inflammatory response requires a better quantitative understanding of how individual immune cells decode pathogen stimulation into effector protein production and how these responses propagate within a highly conserved tissue-level architecture between neighboring immune cells and beyond. Here, using quantitative, single-cell approaches and mathematical modeling, we propose that tissue-level TLR4 signaling

¹Faculty of Biology, Medicine and Health, University of Manchester, Oxford Road, Manchester M13 9PT, UK. ²School of Mathematics, University of Manchester, Manchester M13 9PL, UK. ³Department of Cellular and Molecular Physiology, Institute of Translational Medicine, University of Liverpool, Liverpool L69 3BX, UK. ⁴Department of Chemistry, Centre for Analytical Science, Loughborough University, Loughborough LE11 3TU, UK.

*Corresponding author. Email: pawel.paszek@manchester.ac.uk

involves interactions between different cell types, which regulate local propagation of TNF- α by competitive uptake. In this model, the heterogeneous activation of macrophages by TLR4 results in proximal TNF- α -dependent NF- κ B signaling between neighboring tissue-resident cells but prevents out-of-context TNF- α signaling at longer ranges. We suggest that the tissue-level control of stochastic and spatial interactions between immune cells underlies tissue inflammation.

RESULTS

The macrophage response to TLR4 activation is graded

Tissue-resident macrophages exhibit a highly conserved, grid-like distribution in the central nervous system (29), retina (28), liver (30), and epidermis (31). This distribution may contribute to the propagation of the tissue-level inflammatory response (25). To understand the capacity of cells to produce and propagate antibacterial immune responses (Fig. 1A), we established several cell lines to investigate, by quantified time-lapse microscopy, TLR4-dependent signaling to NF- κ B (38). We generated RAW264.7:Gp65 cells, a macrophage cell line derived from RAW264.7 cells with stable expression of the p65 subunit of NF- κ B fused to enhanced green fluorescent protein (EGFP-p65) and the nuclear marker H2B-mCherry (Fig. 1B and fig. S1A); MEF:Gp65 cells, a mouse embryonic fibroblast (MEF) cell line with stable expression of EGFP-p65 (fig. S1A); and RAW264.7 and MEF lines with stable expression of the NF- κ B reporter encoding nuclear-localized luciferase (RAW264.7: κ B nls-luc and MEF: κ B nls-luc) (fig. S1B). We performed fluorescence correlation spectroscopy (fig. S2A) to convert the EGFP-p65 fluorescence signal into the concentration of NF- κ B (fig. S2, B to E) and calibrated all of the data presented (fig. S2F).

Untreated RAW264.7 cells exhibited a predominantly cytoplasmic localization of EGFP-p65 (Fig. 1, B and C). Stimulation with lipid A, the main cytotoxic component of LPS (39), induced a series of nuclear translocations of the p65 fusion protein, characterized by a robust first peak and then subsequent oscillations with decreasing amplitudes (Fig. 1, B to D, and fig. S3). Individual cell responses were heterogeneous (Fig. 1C) but showed a positive correlation with the stimulation dose (fig. S3 and movies S1 and S2). Using the data from >400 cells for each condition (Fig. 1C), we determined that the response was saturated at higher doses of lipid A (Fig. 1D, AUC graph), that the amplitude of the response increased with dose (Fig. 1D, peak amplitude graph), and that the time to reach the peak decreased and then plateaued (Fig. 1D, time to peak graph). The variability of the single-cell responses substantially decreased upon stimulation, as progressively more cells responded to higher concentrations of lipid A [Fig. 1D, CV² (AUC) and number of responding cells graph]. Together, these results suggest that multiple characteristics of the single-cell responses differed between untreated cells and cells treated with lipid A at concentrations of 10 and 50 ng/ml, whereas the responses to higher concentrations of lipid A were saturated.

In comparison, NF- κ B-dependent transcription, measured with a population-level luciferase reporter gene assay, displayed a much stronger positive correlation with the lipid A dose and did not become saturated (Fig. 1E). Similarly, when measured by quantitative reverse transcription polymerase chain reaction (qRT-PCR) analysis, the increase in mRNA amounts of known NF- κ B gene targets was also dose-dependent (Fig. 1F). These genes include *TNFA*, which encodes TNF- α ; *NFKBIA*, which encodes inhibitor of NF- κ B α ($I\kappa$ B α); *CXCL10*, which encodes C-X-C motif ligand 10 chemokine (CXCL10);

and *NFKB1*, which encodes the NF- κ B subunit p105 (NF- κ B p105) (15). The abundances of mRNAs for *NFKBIA*, which encodes a negative-feedback regulator of NF- κ B dynamics (9), and *TNFA*, which encodes a key effector cytokine, showed up to an 8- and 16-fold change (in comparison with untreated cells), respectively. We also performed secretome analysis of RAW264.7 cells by mass spectrometry (MS), which revealed that TNF- α was one of the most robustly produced cytokines upon lipid A stimulation (fig. S4). The amounts of secreted TNF- α protein correlated with *TNFA* mRNA abundance (Fig. 1G). Thus, the TLR4-induced gene transcription and protein secretion patterns, and to a lesser extent NF- κ B activation in single cells, correlated with the dose of lipid A.

Single-cell expression of *TNFA* is heterogeneous and depends on cell state

To understand the TLR4-induced response in individual macrophages, we used single-molecule mRNA fluorescence in situ hybridization (smFISH) to measure gene transcription (40). To select a time after stimulation for performing smFISH, we performed time-course measurements of *TNFA* mRNA and protein production in wild-type (WT) RAW264.7 cells at 3, 8, and 24 hours after stimulation with lipid A (fig. S5). We found an increase in the amount of TNF- α secreted at 3 hours after stimulation when compared with that secreted at later times (fig. S5, A and B), which was correlated with mRNA abundance as measured by smFISH in single cells (fig. S5, C and D) and qRT-PCR analysis of cellular populations (fig. S5E). From these experiments, we selected 3 hours after lipid A stimulation as the appropriate time for subsequent smFISH analysis of WT RAW264.7 cells. We measured both *TNFA* and *NFKBIA* mRNA abundances in ~1500 cells after 3 hours of stimulation of the cells with different lipid A doses (Fig. 2, A to D). We detected transcripts for *NFKBIA* and *TNFA* in untreated cells: 43 ± 33 transcript molecules for *NFKBIA* and 46 ± 34 for *TNFA*. Treatment with lipid A resulted in a dose-dependent induction of both transcripts (Fig. 2B) of more than three orders of magnitude, with *TNFA* mRNA showing more variability than *NFKBIA* mRNA (Fig. 2C). Despite this heterogeneity, we detected a correlation between *TNFA* and *NFKBIA* mRNA abundance within individual cells, which could result from common regulatory mechanisms (Fig. 2D). Many cells within a population treated with lipid A at a concentration of 500 ng/ml produced a response similar to that of untreated cells (Fig. 2, D and E). Even at the highest dose tested (500 ng/ml), ~35% of cells had transcripts for *TNFA* and *NFKBIA* whose abundances were in the range of those in untreated cells (Fig. 2E). From these results, we propose a model in which the dose of TLR4 stimulus increases the range of the effector cytokine response by activating a subset of cells, rather than by inducing small incremental changes in the response of each cell (Fig. 2F).

Noise analysis provides a method for identifying the source of variability in a data set (41). A decomposition of noise in the data [based on separating the “between” and “within” transcript number variability into “trunk” and “branch” contributions (42)] showed that the observed variability could mainly be attributed to noise occurring in the system at the level of stimulation or the trunk (Fig. 2G). Trunk noise can arise from cells that are in different states, but not stochastic gene regulation; for example, cells may have different amounts of proteins involved in TLR4 signaling or have different rates for biochemical reactions within the NF- κ B system (5, 12, 19). To understand how some cells produced more *TNFA* mRNA than did others, we analyzed the relationship between mRNA number

and cell size (fig. S6). We first defined the boundaries of the cell and the nucleus (fig. S6A) and then the areas for the nuclei and cells for the cells analyzed earlier (Fig. 2) were determined (fig. S6, B and C). Analysis of transcript numbers as a function of nuclear area revealed a positive linear correlation in cells stimulated with a high dose of lipid A (fig. S6D and file S1), which indicated that transcription was increased in larger cells (43). Our analysis showed that ~14% of the

variability in *TNFA* mRNA abundance was related to differences in nuclear size because cellular *TNFA* mRNA abundance after stimulation with lipid A at a concentration of 500 ng/ml changed by 3.1 ± 0.47 -fold and the corresponding nuclear area varied from 70 to 300 mRNA molecules, whereas the remaining 40% of the variability related to differences between the two transcripts (file S1). We performed lipid A dose-response analysis in RAW264.7:Gp65 cells

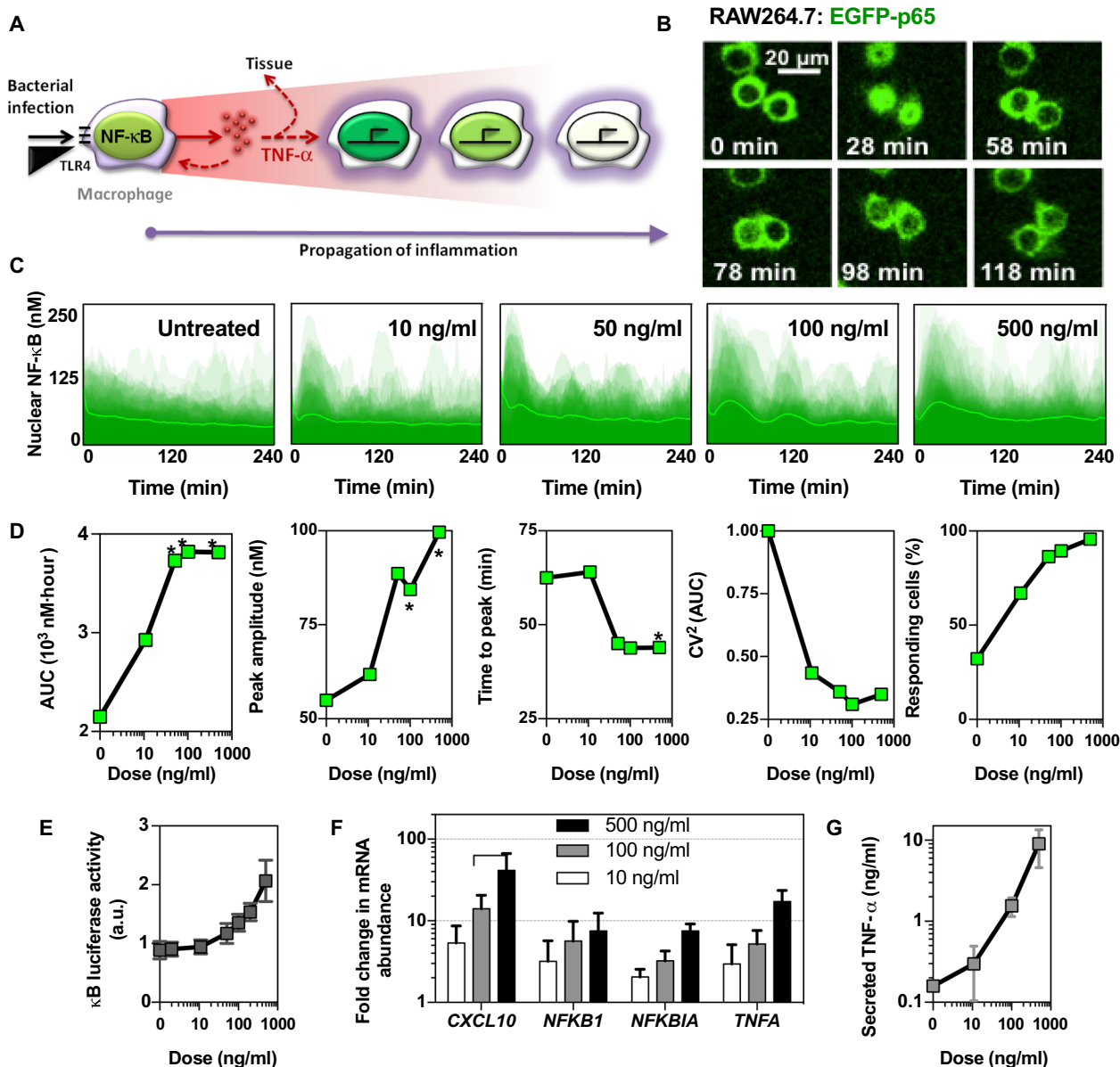


Fig. 1. TLR4-induced macrophage activation is graded. (A) Tissue-level propagation of inflammatory signals: nuclear NF-κB activation (green) and TNF-α production (red) by a single macrophage. (B) Confocal microscopy images of RAW264.7 cells expressing the EGFP-p65 reporter and stimulated with lipid A (500 ng/ml) for the indicated times. (C) Density plots of individual RAW264.7:Gp65 cell traces (total of 432 cells from 91, 76, 59, 87, and 119 cells going from left to right) in response to the indicated lipid A doses (average trajectory indicated by the green line). (D) Analysis of the single-cell traces from (C). Data are mean values of the area under the curve (AUC), maximum peak amplitude and timing, and coefficient of variation (CV) of the AUC of the nuclear NF-κB. The last graph shows the percentage of responding cells. (E) Population-level response of RAW264.7:κB nls-luc cells stably expressing an NF-κB luciferase reporter. Data are means ± SD of triplicate samples per dose of lipid A. a.u., arbitrary units. (F) The NF-κB-dependent production of the indicated mRNAs by RAW264.7 cells stimulated with lipid A (500 ng/ml) for 3 hours was determined by qRT-PCR analysis. Data are means ± SDs of triplicate samples per lipid A dose. (G) The amount of TNF-α in the culture medium of RAW264.7 cells stimulated with the indicated concentrations of lipid A for 3 hours (2.66×10^5 cells in 1 ml) were determined by enzyme-linked immunosorbent assay (ELISA). Data are means ± SD of three replicate experiments per dose of lipid A. * $P < 0.05$ by Kruskal-Wallis analysis of variance (ANOVA) using Dunn's correction for multiple comparisons. In (D) and (F), comparison was made to untreated controls. In all other panels, comparison is as indicated.

(fig. S7, A to C), noise decomposition (fig. S7, D and E), and correlation analysis between mRNA abundance and nuclear size (fig. S7, F and G). In these cells, the difference in nuclear size explained ~37% of the variability (fig. S7H). Together, these data suggest that the activation of macrophages results in an extremely variable TNF- α response, which may in part relate to differences in the size of the nucleus.

The tissue-level *TNFA* response operates in a regime of cytokine consumption

Stimulation of TNF- α secretion may enable propagation of the inflammatory response between resident macrophages (8). We found that TNF- α induced heterogeneous NF- κ B p65 oscillations in RAW264.7:Gp65 cells, in which the response amplitude and per-

centage of responding cells depended on the dose (Fig. 3, A to C; fig. S3; and movie S3). Bone marrow-derived macrophages (BMDMs) from transgenic mice expressing p65-DsRedxp also produced an NF- κ B response when stimulated with TNF- α (Fig. 3, D and E, and fig. S8, A and B) or lipid A (Fig. 3D and fig. S8, A and C to E). Live-cell imaging revealed heterogeneity in the responses of individual cells to each stimulus (Fig. 3E, fig. S8D, and movies S4 and S5). Activation of NF- κ B (as assessed by measuring its nuclear localization) in response to TNF- α or lipid A coincided with a dose-dependent activation of NF- κ B-regulated gene expression, including a statistically significant increase in *TNFA* mRNA abundance (Fig. 3, F and G). Although lipid A induced a statistically significant increase in TNF- α secretion, TNF- α induced only a limited and transient secretion of TNF- α (fig. S8A). Consistent with

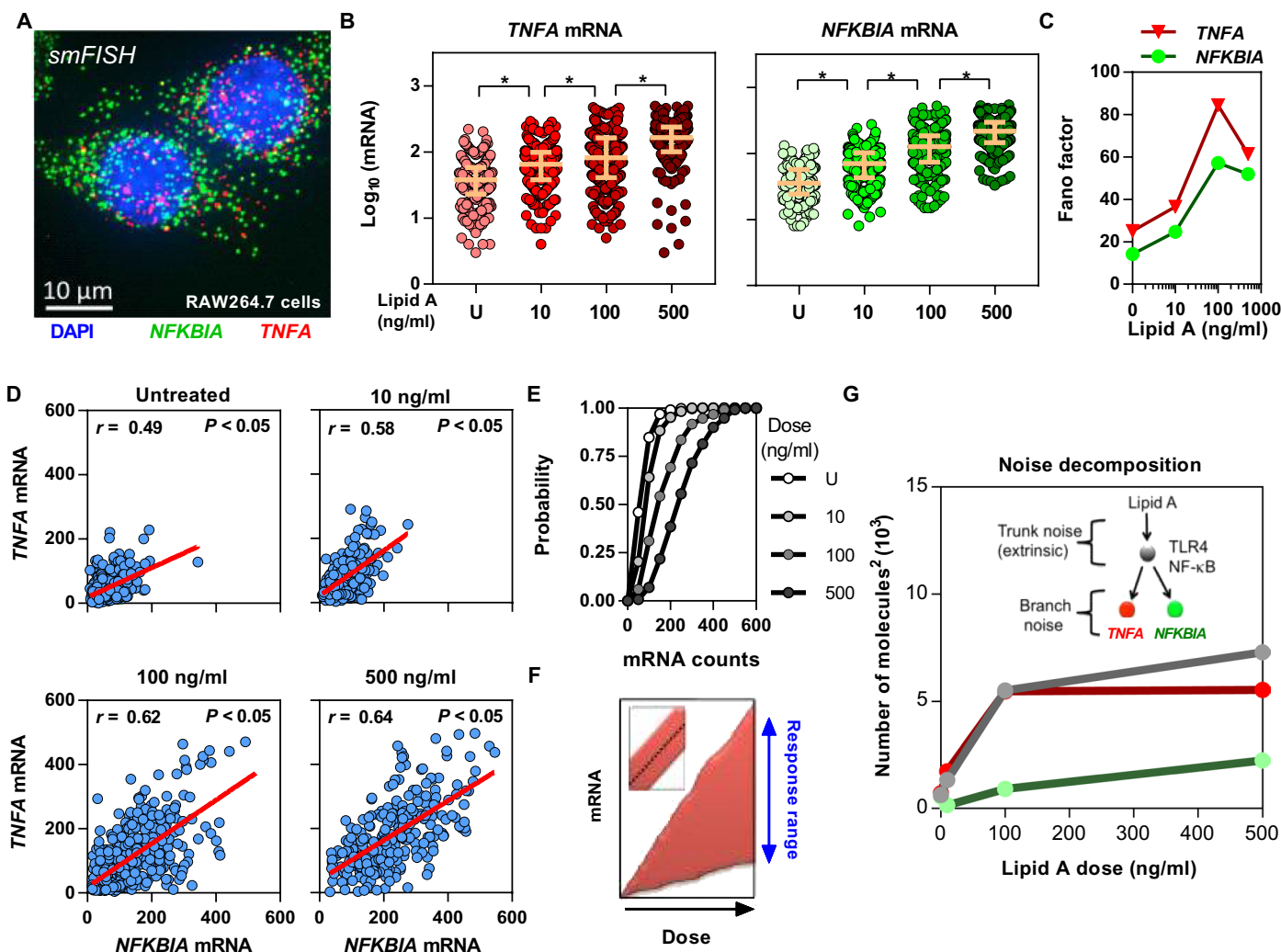


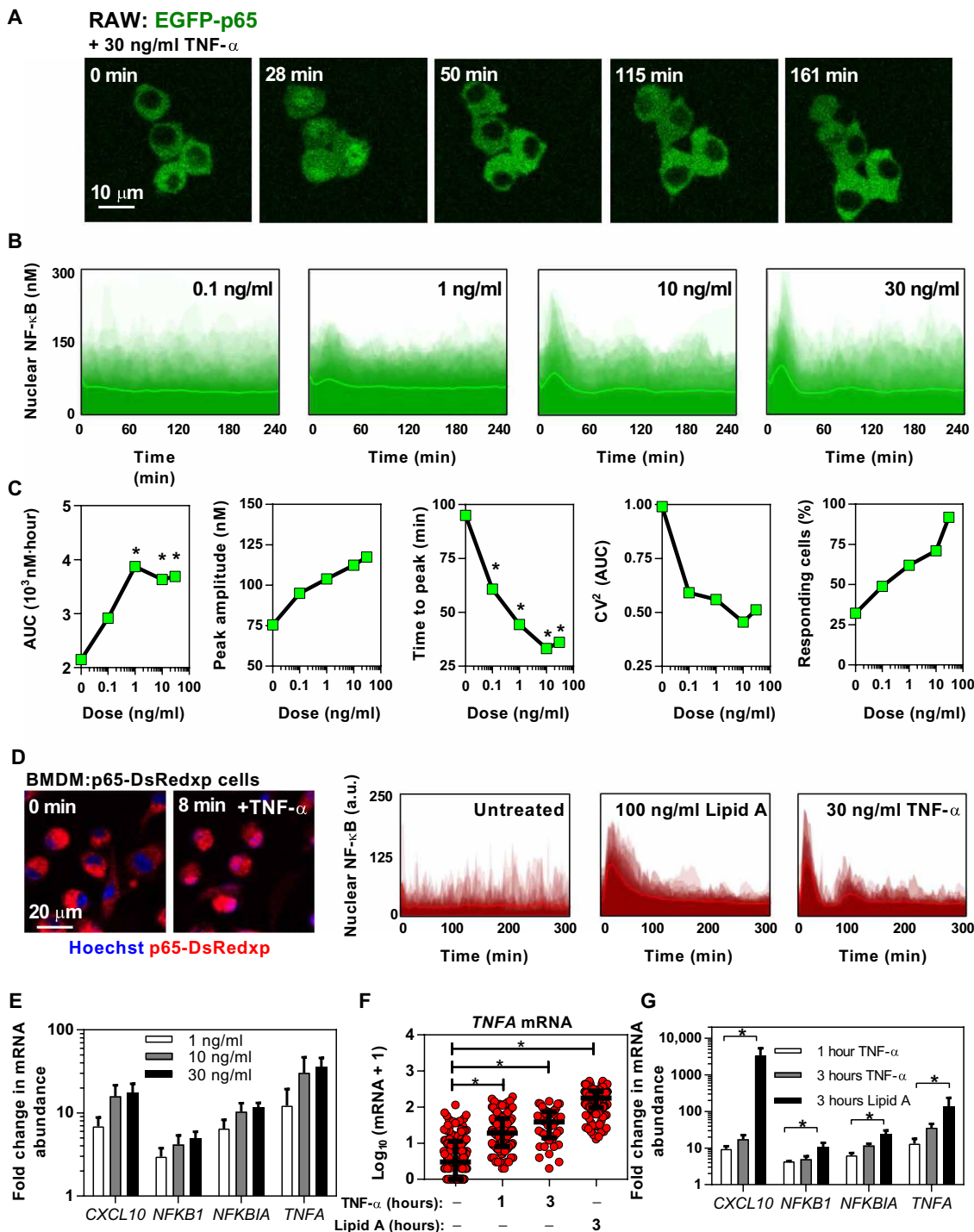
Fig. 2. Heterogeneous *NFKBIA* and *TNFA* mRNA abundance is correlated in single cells. (A) smFISH analysis of *TNFA* and *NFKBIA* mRNA expression. Deconvolved microscopy image of RAW264.7 cells stimulated with lipid A (500 ng/ml) for 3 hours. *TNFA* mRNA is in red, *NFKBIA* mRNA is in green, and 4',6-diamidino-2-phenylindole (DAPI) is in blue. (B) Analysis of the dose-dependent changes in *TNFA* (left) and *NFKBIA* (right) mRNA abundance from the experiments represented in (A). Data are present as \log_{10} , with median and 25% quartiles for a total of 264, 319, 401, and 270 cells pooled from at least three replicate experiments per dose that were untreated (U) or stimulated with lipid A (10, 100, and 500 ng/ml, respectively). * $P < 0.05$ by Kruskal-Wallis ANOVA with Dunn's correction for multiple comparisons. (C) Fano factor calculations of the indicated mRNA numbers from the experiments shown in (B). (D) Correlation between *TNFA* and *NFKBIA* mRNA numbers from the experiments shown in (B) depicted with a fitted regression line and Pearson correlation coefficient r (and associated P value). (E) Joint distribution of mRNA numbers from the data shown in (D). Inset: Constant response range per given dose. (F) Different modes of mRNA regulation: Lipid A dose regulates the range of the response. Inset: Schematics of noise decomposition method. Trunk noise represents extrinsic variability between cells (potentially due to TLR4/NF- κ B signaling or generic gene transcription machinery), whereas branch noise corresponds to gene-specific regulation. (G) Decomposition of noise in the *TNFA* and *NFKBIA* mRNA numbers: extrinsic noise (gray) versus *NFKBIA* (green) and *TNFA* (red) noise. Inset: Schematics of noise decomposition method. Trunk noise represents extrinsic variability between cells (potentially due to TLR4/NF- κ B signaling or generic gene transcription machinery), whereas branch noise corresponds to gene-specific regulation.

previous studies (15, 44), these data suggest that TNF- α may contribute to the propagation of TLR4 signaling between macrophages.

To understand the tissue-level TNF- α response, we used MEFs as a model for nonimmune cells (fig. S1B), which, together with resident macrophages, form the grid-like architecture in the connective

tissue (27). Consistent with previous analyses (12–14), TNF- α stimulated the nuclear translocation of EGFP-p65, indicating NF- κ B activation, in MEFs at doses as low as 100 pg/ml (fig. S9, A to D). Cells expressing the NF- κ B reporter gene showed functional activation of NF- κ B in response to either TNF- α or lipid A (fig. S9, E and F).

Fig. 3. TNF- α activates NF- κ B-mediated signaling in macrophages.



(A) Single-cell analysis of NF- κ B translocation in RAW264.7:Gp65 cells stimulated with TNF- α (30 ng/ml) for the indicated times. Data are confocal microscopy images of the cells showing the EGFP-p65 signal in green. **(B)** Density plots of nuclear NF- κ B trajectories in RAW264.7:Gp65 cells stimulated with the indicated concentrations of lipid A over time. Data are from 91, 131, 108, 83, and 111 cells for untreated cells and cells treated with the indicated concentrations of TNF- α , respectively, and are pooled from at least three replicate experiments. **(C)** Characteristics of the single-cell traces from the data shown in (B). AUC values of nuclear NF- κ B, maximum peak amplitude and timing, the CV of AUC, and the percentage of responding cells to each concentration of lipid A were determined. * $P < 0.05$ by Kruskal-Wallis ANOVA against untreated controls and using Dunn's correction for multiple comparisons. **(D)** Left: Time-lapse microscopy images of BMDM:p65-DsRedxp cells that were treated with TNF- α (30 ng/ml) for the indicated times. NF- κ B p65 is in red, whereas Hoechst nuclear staining is in blue. Right: Corresponding density plots of individual p65-DsRedxp BMDM cell traces across different conditions (average single-cell trajectory in red line). A total of 37 and 39 cells for TNF- α and lipid A stimulation pooled from three replicate experiments were analyzed (49 untreated controls; representative of three replicate experiments). **(E)** WT BMDMs were treated for 3 hours with the indicated concentrations of TNF- α , and the abundances of the indicated mRNAs were then determined by qRT-PCR analysis. Data are means \pm SD of three replicate experiments. **(F)** Analysis of the abundances of the indicated mRNAs in BMDMs that were untreated or treated with TNF- α (30 ng/ml) or lipid A (500 ng/ml) for the indicated times. **(F)** *TNFA* mRNA was measured by smFISH [shown as $\log_{10}(\text{mRNA} + 1)$]. **(G)** The abundances of the indicated mRNAs were measured by qRT-PCR analysis. Data are means \pm SD of three replicate experiments. * $P < 0.05$ by Kruskal-Wallis ANOVA with Dunn's correction for multiple comparisons.

Downloaded from <http://stke.sciencemag.org/> on July 25, 2018

However, in contrast to macrophages, neither TNF- α - nor lipid A-treated MEFs exhibited detectable *TNFA* mRNA production (fig. S9, G and H). The data from our experiments with macrophages and MEFs suggest a one-directional interaction between fibroblasts and macrophages in the TNF- α -mediated inflammatory response: TNF- α -stimulated macrophages may release TNF- α to activate neighboring fibroblasts but not vice versa, which is consistent with a previous study (45). In contrast, we found that a range of epithelial cell lines, which are derived from cells that function as barriers in tissues, had the potential ability to propagate TNF- α signaling (fig. S10). These cells accumulated fluorescently labeled TNF- α (fig. S10, A and B) and produced *TNFA* mRNA in response (fig. S10C).

TNF- α -treated cells internalize this cytokine (19); therefore, we asked whether MEFs might internalize the TNF- α produced by macrophages. We observed internalization of fluorescein isothiocyanate (FITC)-labeled TNF- α by MEFs at 30 min, with total fluorescence increasing roughly linearly—consistent with ongoing, steady uptake—for up to 3 hours after stimulation (Fig. 4, A to C). In contrast, RAW264.7 cells did not accumulate FITC-labeled TNF- α , suggesting that internalization in RAW264.7 cells was much less efficient (Fig. 4, A to C). However, RAW264.7 cells primed with interferon- γ (IFN- γ), a key antibacterial cytokine (46), exhibited a fourfold increase in TNF- α receptor 1 (*TNFR1*) mRNA abundance (compared to that in cells treated with lipid A alone), which was confirmed by flow cytometry analysis (fig. S11, A and B). The increase in *TNFR1* abundance coincided with the increased internalization of labeled TNF- α in RAW 264.7 cells (fig. S11C). Similarly, the amount of TNF- α taken up by MEFs depended on TNFR abundance, and the fluorescent TNF- α signal was reduced in cells in which *TNFR1* was knocked down with short hairpin RNA (shRNA), indicating less internalization (Fig. 4, D to F). In MEFs, but not RAW264.7 cells, treated with recombinant human TNF- α , uptake coincided with a substantial loss of TNF- α from the culture medium (Fig. 4G; see fig. S12, A and B, for calibration curves). Uptake of TNF- α by cells and its concomitant loss from the culture medium depended on cell density (Fig. 4H). We observed a consistent reduction in TNF- α abundance in the medium in lipid A-stimulated cocultures of RAW264.7 cells and MEFs in comparison to the amount in lipid A-stimulated cultures of RAW264.7 cells alone (Fig. 4I).

These data were used to quantify TNF- α production by macrophages (table S1), using concentrations measured by ELISA across the experimental conditions described earlier, experiment-specific cell numbers (with an assumed 24-hour doubling time for RAW 264.7 cells and death rate for BMDMs), and the volume of the culture medium (fig. S12, A and B). This quantification suggests that, on average, a single macrophage may produce up to 1×10^5 TNF- α molecules in 3 hours after stimulation with lipid A (fig. S12C). The large heterogeneity in *TNFA* mRNA production suggests that some of the cells may secrete even larger quantities of protein (21, 47), on the order of 1×10^6 molecules, as was previously suggested (22). We expect that this number is indeed greater not only because of the half-life of TNF- α but also because of the loss of TNF- α due to internalization through its receptor. In parallel, MEFs were used to quantify TNF- α uptake in experiments using ultrasensitive ELISA. A range of experiments (Fig. 4, G to I) showed a loss of TNF- α from the culture medium that corresponded to about 1×10^4 TNF- α molecules per single MEF on average (and ranged between 2000 and 20,000 molecules; see fig. S12C). Given the highly skewed ratio of innate immune cells to other cells in the tissue [of up to 1:50 (25)], these data suggest that the single-macrophage secretion and in vivo tissue uptake rates may be

matched (fig. S12D). Fibroblasts serve as a model for an abundant (nonimmune) cell type in the connective tissue in animals, and they have been widely used to study NF- κ B responses (12, 13, 48). Consistent with our findings, a different fibroblast line (NIH 3T3 cells) shows a limited ability to propagate an inflammatory response (45). However, other fibroblast cell lines (or indeed other tissues) might have different abilities to uptake TNF- α (or potentially other cytokines).

To further characterize TNF- α uptake, we simulated the diffusion of TNF- α in small volumes corresponding to intercellular tissue spaces of different sizes, with 1 pl representing the volume of a single macrophage (38). We assumed that the half-life of TNF- α was 24 hours and then simulated the change in TNF- α half-life as being related to the initial concentration and the size of the intercellular tissue spaces, which we simulated by modeling different concentrations of TNF- α in a range of closed volumes (fig. S13A; see model S1 and tables S2 and S3 for model equations and parameters). Only large quantities of TNF- α (50 nM) resulted in stabilization of the protein. In contrast, low amounts of TNF- α , such as ~ 600 molecules of TNF- α in 1 pl of a 1 nM solution, were effectively removed from the system (fig. S13B). This clearance of TNF- α may depend on internalization by the cognate receptor and degradation of the internalized TNF- α (24, 25). Thus, we simulated the half-life of TNF- α at different amounts of TNFR1 in a model that included receptor internalization and recycling with release and degradation of the internalized TNF- α . At high receptor abundance ($>10^3$ per cell), large quantities of TNF- α were removed from the system, and the simulations predicted that up to 10^4 TNF- α molecules per hour could be removed from the culture medium by a single fibroblast with 2×10^3 TNFRs (fig. S13C). This number of receptors is within the physiological range, because up to 1×10^4 TNFR1 molecules per cell have been measured in different nonimmune cells (49–51), and this predicted uptake rate is consistent with the measured loss of TNF- α from the cell culture medium in the uptake experiments (fig. S12C). Together, these analyses suggest a model of TLR4 signaling in which the amount of TNF- α secreted by macrophages is balanced by consumption of the cytokine through receptor-specific uptake by nonimmune cells in the same tissue.

Computational modeling predicts tissue thresholds for the propagation of TLR4 responses

TNF- α secretion could lead to large concentration gradients in the tissue, resulting in an uncontrolled inflammatory response (32). Our data suggest that, on average, macrophages produce up to 1×10^5 TNF- α molecules within 3 hours of lipid A stimulation (fig. S12C). Given the measured mRNA heterogeneity, this could mean that some cells secrete millions of TNF- α molecules [in agreement with previous single-cell secretion measurements (22)], which then may propagate the signal locally. To quantitatively understand the inflammatory signaling between tissue-resident immune cells, we mathematically modeled the propagation of the TNF- α response between a TLR4-stimulated (TNF- α -producing) cell and target macrophages residing at different distances (Fig. 5A). The TLR4- and TNFR-dependent signaling in macrophages were described by extending our previous models of the NF- κ B system (10, 11, 19) (fig. S14 and tables S2 to S4; see model S2 for description) and fitted to recapitulate the stimulus and dose-dependent NF- κ B dynamics and TNF- α secretion (fig. S15, A to D). We assumed that the abundance of TNFR varied between cells (14) and applied a steady-state approximation for the diffusion of TNF- α through the tissue (34, 35). We accounted for a dense multicellular environment (25) by incorporating high rates of TNF- α

uptake (see table S4 and model S3 for a description). In the model of two interacting cells in which the TNF- α -producing cell was stimulated with lipid A at a concentration of 500 ng/ml, a separation of no more than 40 μ m between the cells was required for robust TNF- α signal propagation (Fig. 5B). This was assessed through the extent of NF- κ B nuclear translocation in the target cell, based on 100 simulated pairs of producing and target cells at different distances apart (assum-

ing a lognormal distribution of TNFR1 across cells). The probability of signal propagation (which we defined as the fraction of responding target cells at a given distance) decreased substantially with separation between the producing and responding cells, falling from ~ 0.75 for separations of up to 40 μ m to 0.1 for a 50- μ m separation (Fig. 5B). For distances greater than 50 μ m, no signal propagation was observed, defining an effective "propagation distance" between resident macrophages

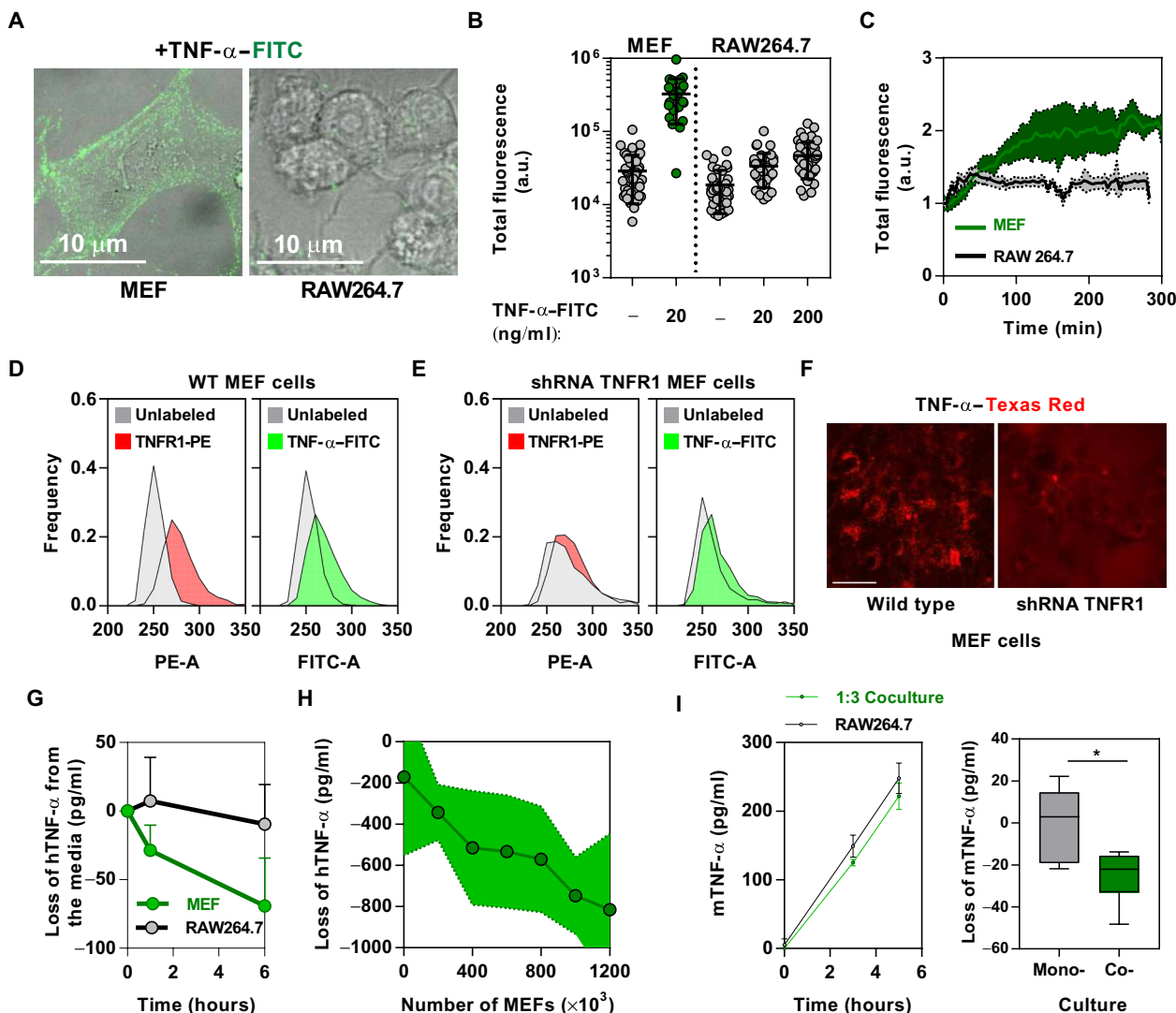


Fig. 4. The amount of available TNF- α is regulated by competitive uptake. (A) Analysis of TNF- α internalization. Representative confocal images of MEFs treated with FITC-TNF- α (20 ng/ml, left) and RAW264.7 cells treated with FITC-TNF- α (20 and 200 ng/ml, right) for 30 min. (B) Analysis of the total cellular fluorescence signal of the cells represented in (A) and treated with the indicated concentrations of FITC-TNF- α . Data are means \pm SD of three replicate experiments. (C) Time-lapse microscopy analysis of TNF- α internalization. Data are means \pm SD of the total fluorescence in MEFs ($n = 10$) and RAW264.7 cells ($n = 13$) treated for the indicated times with FITC-TNF- α (30 ng/ml). (D and E) Flow cytometry analysis of FITC-TNF- α internalization and TNFR1 abundance [with phycoerythrin (PE)-labeled antibody] for WT MEFs (D) and TNFR1 knock-down MEFs (E) treated with FITC-TNF- α (10 ng/ml). (F) Confocal microscopy image of WT and TNFR1 knockdown MEFs treated with Texas Red-labeled TNF- α (30 ng/ml). (G) Analysis of the loss of mouse TNF- α (mTNF- α ; pg/ml) from the culture medium of RAW264.7 cells or MEFs (5×10^4 cells in 1 ml) treated with human TNF- α (hTNF- α ; 1 ng/ml). Cell culture medium was assayed by ultrasensitive ELISA at the indicated times. Data are means \pm SD of three replicate experiments. (H) Loss of TNF- α from the culture medium is cell density-dependent. A range of MEF densities were simulated experimentally by passing the culture medium across one and up to a total of six cell cultures (each with 2×10^5 cells in 1 ml) every 10 min. The initial culture was stimulated with human TNF- α (1 ng/ml). Zero density indicates no cell control (passed over six different cell-free dishes). The amount of human TNF- α after each step was measured by ultrasensitive ELISA. Data are means \pm SD of three replicate experiments. (I) Loss of lipid A-induced TNF- α in the coculture medium of RAW264.7 cells and MEFs. Cocultured RAW264.7 cells and MEFs or RAW264.7 cells alone were stimulated for the indicated times with lipid A (500 ng/ml) before the concentration of TNF- α in the culture medium was measured by ultrasensitive ELISA. For the coculture experiments, a 1:3 ratio of RAW264.7 cells (5×10^4 cells) to MEFs (1.5×10^5 cells) in 1 ml of medium was used. Left: Time-course experiments. Data are means \pm SD of three replicate experiments. Right: Pooled individual data points. * $P < 0.05$ by Mann-Whitney test.

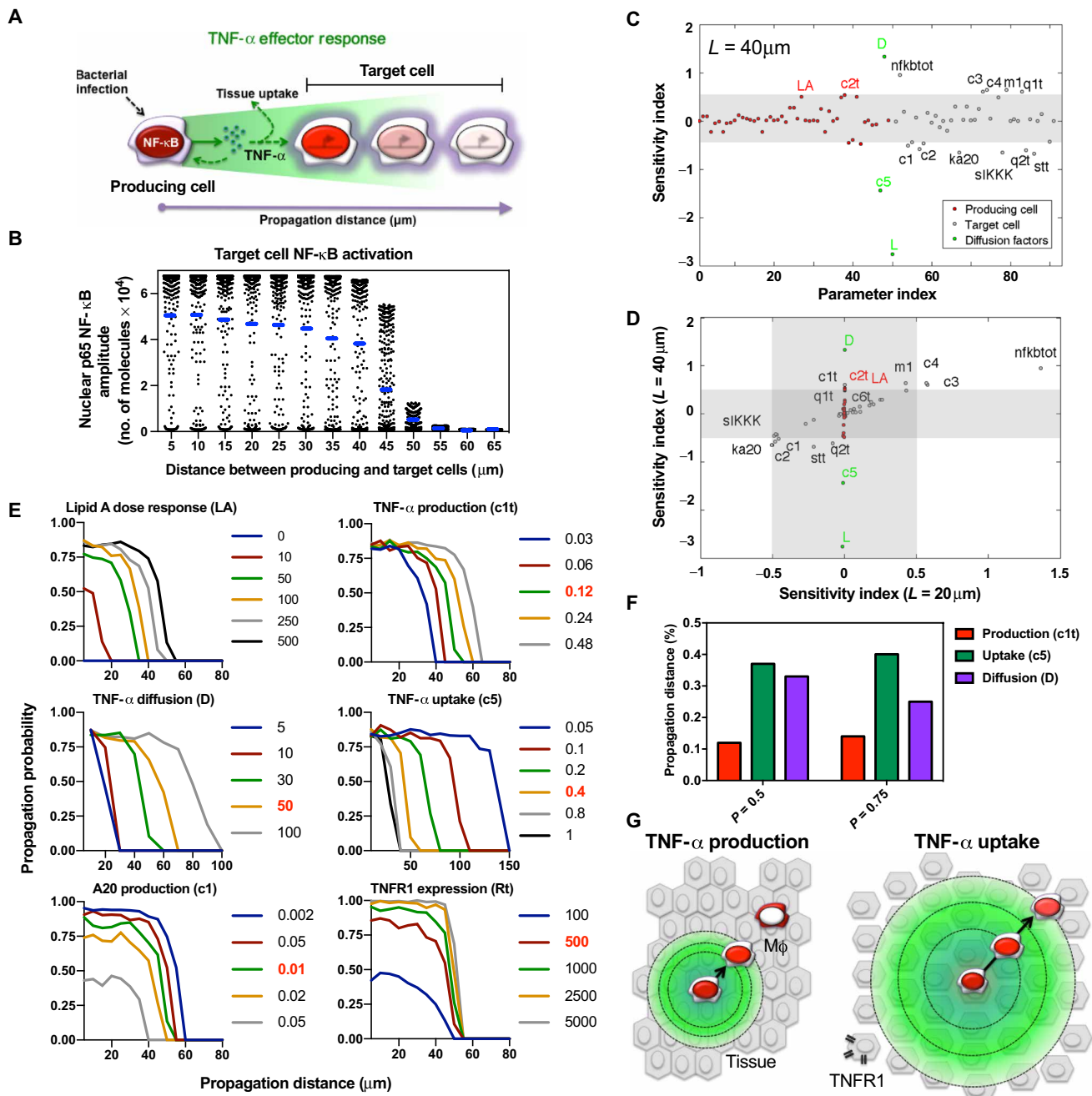


Fig. 5. TLR4 signal propagation is restricted in the tissue. (A) Two-cell model of tissue-level macrophage signaling. Lipid A activates the secretion of TNF- α by a producing cell. TNF- α can activate a receiving cell but can also be removed by competitive uptake. (B) Distribution of first-peak nuclear NF- κ B amplitude in a receiving cell at different distances from the producing cell. We performed 100 simulations with lipid A (500 ng/ml) at each of the indicated distances. TNFR1 abundance was distributed lognormally with a mean of 500; mean TNFR1 abundance is shown in blue. (C) Global sensitivity analysis of the two-cell model. The sensitivity index was calculated with respect to the AUC of nuclear NF- κ B in a receiving cell 40 μ m from the producing cell. The producing cell was stimulated with lipid A (500 ng/ml) for 3 hours. We assumed the mean TNFR1 abundance on the receiving cells. Parameters describing the producing and target cells are shown in red and gray, respectively. Spatial parameters corresponding to TNF- α diffusion are shown in green. Sensitivity index values < -0.5 and > 0.5 are indicated by the gray area. (D) Correlation between the sensitivity indexes calculated for distances of 20 and 40 μ m. Simulations were performed as described in (C). (E) The probability of TNF- α signal propagation depends on system parameters. The probability of signal propagation was calculated for changes in TNF- α uptake (c5), production (c1t), diffusion (D), as well as target cell TNFR1 receptor abundance (Rt) and A20 transcription (c1). Nominal parameter values are indicated in red. Activation was defined by a first-peak nuclear NF- κ B amplitude $> 10^4$ molecules across 300 cells simulated for each distance. Producing cells were stimulated with lipid A (500 ng/ml) for 180 min. Receiving cell TNFR1 abundance was distributed lognormally with a mean equal to Rt. (F) Propagation distance depends on tissue thresholds. A local sensitivity analysis of the propagation distance with respect to TNF- α transcription (c1t), as well as tissue uptake (c5) and diffusion (D), is shown. Sensitivity was calculated on the basis of the data in (E) by averaging the changes in distance versus twofold parameter changes (up and down, in comparison to the nominal parameter values). Distances were calculated for 0.5 and 0.75 propagation probability (P). (G) Schematics of the proposed tissue-level signaling: TLR4 signal propagation depends on the competitive uptake of TNF- α (right), rather than on the variability in the TLR4-induced production of TNF- α (left).

in the tissue. This analysis therefore predicted that TLR signal propagation is restricted locally, which our experiments indicated was achieved by matched TNF- α production and uptake rates (fig. S12D).

To quantitatively understand the relationship between the model parameters and the observed patterns of spatial signaling, we used a suite of sensitivity analysis tools (see the “Mathematical modeling” section in Materials and Methods). Global sensitivity analyses (52) indicated that, at larger distances (40 μ m and greater), the generic target cell NF- κ B response depended on parameters related to TNF- α production, transport, and uptake [Fig. 5C; TNF- α production (c_5t), lipid A dose (LA), diffusion rate (D), and TNF- α uptake (c_5)]. In contrast, at short distances (thus, with higher local TNF- α abundance), responses were controlled by parameters of the NF- κ B system activity in the target cell (Fig. 5D). We performed simulations to understand how the key system parameters identified by global sensitivity analyses and those from the experiments affected the spatial signal propagation (Fig. 5E and see model S3 for details). We found that the parameters associated with TNF- α production (as simulated with the transcription rate c_1t varied over 16-fold, or dose of stimulation; fig. S15, E and F), as well as tissue uptake and diffusion, robustly regulated the propagation distance. However, even the largest parameter changes (for example, 20-fold changes in TNF- α uptake or diffusion) resulted in localized responses, consistent with steep TNF- α concentration gradients (36). In contrast, parameters associated with target cell state—such as TNFR1 abundance, which is increased in disease states (18) or by prestimulation with IFN- γ , leading to enhanced NF- κ B activity (fig. S16, A and B; see also model S4)—or NF- κ B system sensitivity, which we modeled by A20 feedback (see model S1), did not affect propagation distance but instead increased the probability of signal propagation between neighboring macrophages (Fig. 5E).

Our single-cell data indicate that individual macrophages secrete widely different amounts of TNF- α , which ultimately could affect the propagation distance (36, 37). We therefore directly calculated the effect of varied TNF- α production on the signal propagation in relation to parameters related to tissue architecture, TNF- α uptake, and diffusion. We found that the twofold changes in the rate of *TNFA* transcription, which were the magnitude of the observed cell-size effect (fig. S6), resulted in a ~10% change in the propagation distance (Fig. 5F), which we defined as a distance equivalent to the 0.5 and 0.75 propagation probability (Fig. 5E). In contrast, equivalent changes of tissue architecture resulted in ~40% changes in the propagation distance. These results suggest that the range of TLR4 signal propagation may be controlled through competitive uptake of TNF- α , rather than through variability in the TLR4-induced production of TNF- α (Fig. 5G).

DISCUSSION

Here, we investigated the activation and propagation of the TLR4 effector response in highly constrained tissue environments (Fig. 1A), which involve matrices of resident innate immune cells, spatially isolated through nonimmune cells (26). First, we used time-lapse microscopy and quantitative mRNA FISH to characterize the TLR4-dependent activation of NF- κ B signaling and *TNFA* mRNA production in single RAW264.7 cells. We observed dampened NF- κ B p65 nuclear-to-cytoplasmic oscillations in response to the TLR4 agonist lipid A in macrophages (Fig. 1). The NF- κ B response appeared to be graded in single cells, as was previously suggested (3), in contrast to the digital encoding observed in other nonimmune cell types (13, 14). Furthermore, in macrophages, we found only a limited correlation

between the single-cell NF- κ B p65 response and the dose of stimulus (3–5). This corresponded to up to ~2-fold changes in the range of response characteristics. In contrast, the dynamic range of the corresponding population-level mRNA changes was much wider (almost 18-fold for *TNFA* mRNA). The graded mRNA patterns in a cellular population (Fig. 1) resulted from extremely variable *NFKBIA* and *TNFA* mRNA responses, with mRNA abundance changes spanning three orders of magnitude (Fig. 2). The dynamical range of the average single-cell mRNA response was higher than that of the NF- κ B dynamics (for example, a fourfold change for *TNFA*), suggesting a role for other NF- κ B members (8) or other transcription factors (53) in the process. The abundance of *NFKBIA* and *TNFA* transcripts was highly correlated within single cells (Fig. 2), consistent with an extrinsic noise in the system (5, 12). We found that a part of the heterogeneity could be explained by the size of the cell, with larger cells producing more *TNFA* mRNA. This relationship might result from global transcriptional mechanisms, which couple mRNA transcription with the cellular volume (43), in part contributed to the signal-specific regulation of macrophage morphology (54). This mechanism might also involve maintenance of the cellular NF- κ B concentration independently of the cell size, as we previously observed (38). Alternative mechanisms might involve a specific gating of the inflammatory response through the cell cycle system, for example, through modulation of NF- κ B dynamics (55). Further studies will be required to understand precisely how the observed target gene expression (and protein secretion) correlates with heterogeneous NF- κ B dynamics in single cells (56) and how it is influenced by other factors, for example, potential augmentation of the TLR response through paracrine or autocrine signaling (20, 21). Furthermore, the observed variability of TNF- α production (and NF- κ B signaling) suggests that isolated immune cells involved in an early response might have very different capacities to produce and amplify the inflammatory response.

TLR-mediated macrophage activation, for example, during pathogen infection, such as by *Salmonella enterica* (57), may result in the localized production of large quantities of TNF- α (Fig. 1G and fig. S5). This could lead to uncontrolled propagation of inflammatory signaling between immune cells and ultimately result in septic shock (58). One strategy that cells use to neutralize such high amounts of TNF- α involves TNFR shedding (59), and we indeed observed shed TNFR2 in the proteomic analysis of lipid A-stimulated macrophages (fig. S4). Additionally, amplification of the TNF- α response by macrophages might also require additional contextual signaling, which is required to activate protein secretion (22, 60). Here, we showed that MEFs, a model of a nonimmune constituent of connective tissue, might consume large amounts of TNF- α (having a limited ability to produce TNF- α themselves). This suggests a one-directional signal propagation from macrophages to nonimmune cells, which is consistent with another study (45). We also showed that TNF- α uptake involved internalization of the cytokine by TNRF1 (Fig. 4). This finding emphasizes a dual purpose for TNFR1, in which TNFR1 both mediates proinflammatory NF- κ B signaling and acts in an anti-inflammatory capacity by removing localized TNF- α . Thus, changes to the cellular abundance of TNFR1 may contribute to inflammatory disease states. In the mathematical model, it was assumed that TNF- α removal depends on TNFR1 abundance, which was represented by a single receptor species. We suggest that the measured abundance of TNFR1 (between 1×10^3 and 1×10^4 receptors per cell) would be consistent with this behavior (49–51); however, the potential contribution of TNFR2 signaling cannot be excluded. Together, our data

suggest that the tissue-level TNF- α effector response is restricted by cytokine consumption, similar to the cytokines involved in adaptive immunity (23, 34, 37).

Previous analyses linked cellular heterogeneity with population-level robustness (11, 20, 23, 24); however, the earliest stages of the immune response may involve spatially isolated immune cells (26), which could make these responses more susceptible to noise. On the basis of our *in vitro* data, we mathematically modeled early inflammatory events *in vivo*, in which a resident macrophage becomes activated by a pathogen (corresponding to a lipid A stimulation) and locally produces large amounts of TNF- α , which can potentially diffuse and activate neighboring resident macrophages (Fig. 5). We found that competitive TNF- α uptake restricted the range of TLR4 signaling to small distances (<50 μ m), enabling interactions between neighboring immune cells. This is essentially a consequence of matched production and uptake rates in a local environment (fig. S12) because of the highly skewed ratio between immune (TNF- α -producing) and nonimmune (TNF- α -consuming) cells *in vivo* (25). These predictions are consistent with existing *in vitro* microfluidic data, which demonstrate that a single macrophage may locally control the NF- κ B responses of ~100 fibroblast cells (45). We showed that the presence of priming signals affecting TNFR abundance (fig. S11), for example, due to priming by LPS or IFN- γ (46) or disease state (18), regulated the probability of signal propagation between resident cells, whereas parameters associated with TNF- α signaling affected the interaction distance. Of the latter, we showed that the tissue architecture (modeled through TNF- α uptake and diffusion) rather than the variability of TNF- α production had the most profound effect on the signaling range (Fig. 5F). This suggests that spatial signaling effectively minimizes the effect of the single-cell heterogeneity and cellular noise in TLR4 activation (including the effect attributed to cell size). In contrast, the tissue architecture characterized by varied cell densities and intercellular distances (Fig. 1A) would have a more profound effect on the signaling range, potentially leading to tissue-specific patterns. In summary, we propose that competitive cytokine uptake in a local tissue enables signal propagation between neighboring tissue-resident immune cells while restricting longer-range activation and inappropriate signaling. This mechanism would effectively mimic a highly localized cell activation paradigm similar to that achieved in adaptive immunity (33–35). One way to test these ideas would be an application of intravital imaging (33) or advanced microfluidics (45), which could enable direct studies of cellular communication in the primary tissue or *in vitro*. We suggest that spatial TLR4 signaling might be a highly regulated and versatile process. Further studies are required to understand more complex physiological scenarios, including multiple infections, altered macrophage density during infection or in the disease state (26), as well as potential distinct uptake characteristics of different tissue cells. For example, we showed that epithelial cells have the potential to propagate cytokine signaling, which might be important in signal propagation through barrier surfaces (fig. S10). We hypothesize that the tissue-level control of stochastic interactions between innate immune cells might represent a key mechanism underlying contextual propagation and amplification of cellular inflammation.

MATERIALS AND METHODS

Reagents

RAW264.7 cells (a mouse macrophage cell line) and MEFs were cultured as previously described (38). CMT 93 (ECACC 89111413) mouse

rectal carcinoma epithelial cells were grown in high-glucose Dulbecco's modified Eagle's medium (DMEM) (Sigma-Aldrich, D5796-500ml) supplemented with 10% fetal calf serum and 1% nonessential amino acids (NEAAs). HeLa human cervical cancer cells were grown in MEM (Sigma-Aldrich, M4655-500ml) supplemented with 10% fetal calf serum and 1% NEAAs. MCF7 human breast adenocarcinoma epithelial-like cells were grown in DMEM/F12 (Gibco, 11320-074) supplemented with 10% fetal calf serum. All cell lines were subcultured every 2 to 3 days using appropriate split ratios (~1:5 to 1:7). Cells were stimulated with lipid A *Salmonella minnesota* Re595 (VWR), recombinant mouse TNF- α (Calbiochem), or recombinant mouse IFN- γ (Life Technologies). Biotinylated TNF- α (human recombinant TNF- α biotin conjugate; Fluorokine, R&D Systems) was used for internalization studies. Hoechst 33342 (Life Technologies) staining was used to visualize the nuclei of BMDMs to assist in imaging analysis.

Transduced and primary cells

Lentiviral transduction (38) was used to produce RAW264.7 (termed RAW264.7:Gp65) and MEF (MEF:Gp65) cell lines stably expressing the NF- κ B EGFP-p65 fusion protein (fig. S1) (14). RAW264.7:Gp65 cells also expressed an H2B-mCherry nuclear marker (38). NF- κ B transcriptional activity was monitored with a lentiviral construct (κ B-NLSluc), which includes a 5 \times κ B consensus promoter regulating a sensitive and destabilized firefly luciferase reporter gene as previously described (61). Knockdown of TNFR1 abundance was achieved with the pGFP-TNFRSF1a-B lentiviral shRNA vector (OriGene). Primary BMDMs were differentiated from bone marrow taken from the hind legs of adult C57BL/6 NF- κ B reporter mice. Isolated cells were disrupted and homogenized by repeated pipetting until no lumps were visible. The cell suspension was then centrifuged at 200g for 5 min, and the resulting pellet was resuspended in DMEM supplemented with penicillin (100 U/ml), streptomycin (100 μ g/ml) (both from Sigma-Aldrich), 10% fetal calf serum (Gibco), and 30% L929 cell-conditioned medium and then were plated. After 72 hours, the medium was replaced with fresh supplemented medium. Cells were harvested by washing with cold phosphate-buffered saline (PBS) on days 6 to 8 and were used for experiments within 24 hours.

NF- κ B reporter mice

We used BMDMs from mice expressing the previously described I κ B α -EGFP (19) and p65-DsRedxp (55) bacterial artificial chromosome (BAC) constructs. To generate transgenic mice, the p65-DsRedxp BAC was maxi-prepped (NucleoBond BAC 100), and fresh BAC DNA was digested with Asc I to linearize the construct. The digested DNA was purified by Sepharose column purification as previously described (62) in injection buffer [10 mM Tris (pH 7.5), 0.1 mM EDTA (pH 8.0), and 100 mM NaCl]. Positive fractions for DNA were quantified and supplied to the Max Planck Institute of Molecular Cell Biology and Genetics, Dresden, Germany, for microinjection (at 1 ng/ μ l) into 1-day-old, single-cell C57BL/6 mouse embryos. Zygotes were cultured and surgically implanted into the oviducts of day 0.5 postcoital pseudopregnant mice. A single founder was identified using primers targeting the DsRedxp sequences. For I κ B α -EGFP BAC mice, the process was repeated with linearization achieved by digestion with Not I and genotyping of the founders with primers against the EGFP sequence. Mice were then crossed, and cells from animals expressing both constructs were subsequently analyzed by microscopy.

Single-molecule RNA-FISH

Custom Stellaris FISH Probes were designed against murine *TNFA* (accession number NM_001278601) and *NFKB1A* (NM_010907) as well as human *TNFA* (Ensembl ENSG00000232810|ENST00000449264) complementary DNA (cDNA) by using the Stellaris FISH Probe Designer (Biosearch Technologies Inc.). Two probe designs were used for mouse *TNFA*: Design 1 was used in fig. S4, whereas design 2 was used for all other experiments (see file S1 for a list of probes). The *NFKB1A* and *TNFA* probes were conjugated with the Quasar 570 and Quasar 670 dyes, respectively. Samples were imaged with a DeltaVision (Applied Precision) wide-field microscope with a 60×/NA (numerical aperture) 1.42 oil immersion Plan Apo N objective, and a Sedat Quad filter set was used. The images were collected with a CoolSNAP HQ (Photometrics) camera with a *z* optical spacing of 0.2 μm. Raw images were deconvolved using softWoRx software. Spot counting was performed with FISH-quant (40). The total cell area was calculated by extracting the number of pixels and pixel size in each drawn cell boundary. The nuclear area was calculated by applying the MATLAB function “greytresh” to the maximum projection of the deconvolved DAPI signal. Pixel areas for each nuclear mask were extracted and scaled to the actual pixel sizes. Noise decomposition of mRNA count data was performed as previously described (42).

Confocal microscopy

Cells were plated onto 35-mm glass-bottomed dishes (Greiner Bio-One) and incubated on the microscope stage at 37°C in humidified 5% CO₂. Several Zeiss confocal microscopes were used (LSM Pascal, Exciter, 510meta, 710, and 780), which used either dichroic mirrors and band-pass filters or spectral separation or detector arrays to collect appropriate emission signals after excitation of the fluorophore with the appropriate laser. Image capture was performed with the Zeiss software, either “Aim version 4.2 utilizing the Autofocus macro” (63) on the five-series microscopes or “Zen 2010b SP1” on the seven-series microscopes. A range of objectives was used: Fluar 20× NA 0.75 (air), Fluar 40× NA 1.3 (oil immersion), and Plan-Apochromat 63× NA 1.4 and 100× NA 1.46 (oil immersion). Cell Tracker (version 0.6) was used to quantify time-lapse confocal images (64). The MATLAB function “clustergram” was used for clustering analysis.

Fluorescence correlation spectroscopy-calibrated imaging

To quantify fluorescent time-lapse live-cell imaging data, fluorescence correlation spectroscopy (FCS) was applied as previously described (38). FCS measurements were performed in the cytoplasm for one to five cells per imaging location, yielding a range of molecule concentrations (per confocal volume) for each of the cell lines (fig. S2). This FCS-measured distribution was then used to calibrate time-lapse imaging data by quantile-quantile matching to the respective fluorescence signal distribution obtained in a different experiment. This process enabled absolute nanomolar quantification of the intracellular localization of nuclear NF-κB p65 fusion over time (fig. S2).

Enzyme-linked immunosorbent assay

The ultrasensitive mouse and human R&D Systems Quantikine Kits were used in all analyses of TNF-α uptake (see table S1 and fig. S12, A and B). In monoculture studies, cells were treated with human TNF-α, and the loss was measured by assaying the culture medium over time. In coculture experiments, the abundance of mouse TNF-α was measured. Otherwise, the R&D DuoSet (with a wider dynamical range) was used to measure TNF-α production. Cell culture medium

was stored at –80°C. Subsequently, the samples were thawed and diluted to within the dynamic range of the assay, and TNF-α concentrations were measured according to the manufacturer’s instructions.

Live-cell luminometry

Cells were plated into 24-well white plates (PerkinElmer Inc.) in 1 ml of medium containing luciferin (0.5 mM, Biosynth AG). Live-cell measurements were made with a FLUOstar Omega microplate reader with an attached incubator to maintain the cells at 37°C and 5% CO₂. Individual wells were measured every 10 min with an 8-s integration time for up to 24 hours. Because of the low luminescence signal at time zero, data were normalized to the population average of the final time point.

Evaluation of TNF-α internalization

Both MEFs and RAW264.7 cells were imaged during stimulation with labeled TNF-α as previously described (19). Briefly, human recombinant TNF-α-biotin (5 μg/ml; Fluorokine, R&D Systems) was incubated in the presence of either avidin-FITC (10 μg/ml; Fluorokine, R&D Systems) or avidin-Texas Red (2 mg/ml, Life Technologies). Labeled TNF-α was then used to treat either MEFs or RAW264.7 cells at different concentrations. Cells were imaged by *z*-stack confocal microscopy (as outlined earlier) as single images between 30 and 45 min after stimulation or as time lapse.

Flow cytometry

Cells were plated and then treated with TNF-α, conjugated TNF-α, or IFN-γ. After the appropriate incubation time, cells were collected into a suspension. RAW264.7 cells were scraped into suspension, whereas MEFs were removed by washing with PBS. Cells were then fixed by treatment with 3.75% paraformaldehyde for 10 min, after which the cells were centrifuged for a second time and resuspended in 1× PBS. For receptor labeling, cells were incubated with mouse anti-TNFR1 antibody conjugated with PE (2 μg/ml, BioLegend). Cells were washed with 1× PBS to ensure removal of unbound antibody mix and then resuspended in 500 μl of PBS for analysis. Samples were analyzed using either a BD FACSCalibur flow cytometer or a FACSVerse flow cytometer (BD Biosciences) using a 488-nm laser to excite PE. Fluorescence was detected with an appropriate band-pass filter.

qRT-PCR analysis

Cells were plated in 35-mm tissue culture dishes (266,000 cells per dish). At appropriate times after stimulation, total RNA was extracted from the cells with the High Pure RNA Isolation kit (Roche) according to the manufacturer’s instructions and quantified with a NanoDrop ND-1000 Spectrophotometer (Thermo Fisher Scientific). RNA (1 μg) was reverse-transcribed and amplified with the SuperScript VILO cDNA synthesis kit (Life Technologies). For qRT-PCR, cDNA was diluted 1:20 (or 1:10 for BMDM samples) with ribonuclease-free, diethyl pyrocarbonate-treated water and amplified using the LightCycler 480 SYBR Green 1 Master Mix (Roche). Experiments were performed in triplicate. Relative quantification of mRNA abundance was conducted using *Cyclophilin A* mRNA abundance as an endogenous control. The sequences of the primers used are as follows (5′ to 3′): *NFKB1A*, GTGTAGCAGTCTTGACGCAG (forward) and CATCAGCACCCAAAGTCACC (reverse); *CXCL10*, GCCGTCATTTTCTG-CCTCAT (forward) and GATAGGCTCGCAGGGATGAT (reverse); *NFKB1*, TGGCAGACGATGATCCCTAC (forward) and CCCCTCT-GTTTTGGTTGCTC (reverse); *TNFA*, TGAGGTCAATCTGCCAAGT

(forward) and TGGACCCTGAGCCATAATCC (reverse); *Cyclophilin A*, CTGGACCAAACACAAACGGT (forward) and TGCCCCGAAGT-CAAAAGAAA (reverse).

Proteomics analysis

All chemicals used were from Sigma-Aldrich unless otherwise stated. Three controls and five supernatant samples stimulated with lipid A (500 ng/ml) for 3 hours were digested according to the filter-aided sample preparation method (65) with the following modification: The samples were concentrated to about 50 μ l with Microcon-10kDa centrifugal filter units (Merck Millipore) at 14,000g. The sample was then buffer-exchanged by washing and centrifuging three times with the addition of 100 μ l of 25 mM ammonium bicarbonate before reconstitution in 50 μ l of 25 mM ammonium bicarbonate. The protein concentration was determined with a Millipore Direct Detect spectrometer, and 50 μ g of protein was added to a fresh 10-kDa filter tube with reduction, alkylation, and digestion occurring using the filter tubes. Digested peptides were collected by centrifugation and desalted with OLIGO R3 reversed-phase media on a microplate system and reconstituted in 5% acetonitrile and 0.1% formic acid. Digested samples were analyzed by liquid chromatography–tandem MS (LC-MS/MS) with an UltiMate 3000 Rapid Separation LC (RSLC, Dionex Corporation) coupled to an Orbitrap Elite mass spectrometer (Thermo Fisher Scientific). Peptide mixtures were separated using a gradient from 92% A (0.1% formic acid in water) and 8% B (0.1% formic acid in acetonitrile) to 33% B, in 44 min at a rate of 300 nL/min with a 250 mm \times 75 μ m (inner diameter), 1.7 mM BEH C18 analytical column (Waters). Peptides were selected for fragmentation automatically by data-dependent analysis. The acquired MS data were analyzed with Progenesis LC-MS (v4.1, Nonlinear Dynamics). The retention times of each sample were aligned using one LC-MS run as a reference; then, the “Automatic Alignment” algorithm was used to generate maximal overlay of the two-dimensional feature maps. Features with charges $\geq +5$ were masked and excluded from further analyses, as were features with <3 isotope peaks. The resulting peak lists were searched against the UniProt Mouse database (version 2013 -5) using Mascot v2.4 (Matrix Science). Search parameters included a precursor tolerance of 5 parts per million and a fragment tolerance of 0.5 Da. Enzyme specificity was set to trypsin, and one missed cleavage was allowed. Carbamidomethyl modification of cysteine was set as a fixed modification, whereas methionine oxidation was set to variable. The Mascot results were imported into Progenesis LC-MS for annotation of peptide peaks and statistical analysis (66). The proteomics data are deposited with the ProteomeXchange Consortium (67) through the PRIDE repository with the data set identifier PXD001905 and 10.6019/PXD001905.

NanoString analysis

Total RNA was extracted from WT RAW 264.7 cells with the Roche High Pure RNA Isolation Kit. The nCounter Gene Expression assay (NanoString Technologies) was performed according to the manufacturer’s instructions. Transcript numbers were normalized to the relevant housekeeping genes using the NanoStringNorm package within Bioconductor (68). The geometric mean was used to summarize the positive (CodeCount) and housekeeping controls, with a stringent background correction applied (mean \pm 2 SDs).

Mathematical modeling

We considered propagation of TNF- α between a donor (lipid A-stimulated) and target macrophage in a tissue environment (Fig. 5).

Cells were positioned at both ends of a tube of finite volume with plane, parallel surfaces enabling secreted TNF- α to diffuse within the volume (34). Lipid A-induced NF- κ B activation (and TNF- α secretion) in a producing cell and TNF- α -induced NF- κ B activation in the target cell were considered. Single-cell models of the NF- κ B system (10, 11) were extended to model TLR4 and TNFR activation in macrophages. The extended models recapitulated (i) single-cell NF- κ B responses to lipid A and TNF- α stimulation, (ii) dose-dependent smFISH measurements of average *NFKBIA* and *TNFA* mRNA abundance, (iii) TNF- α secretion, and (iv) TNF- α uptake by nonimmune cells. Cellular heterogeneity was modeled by randomly distributed TNFR abundance across cells or by variation in the *TNFA* transcription rate. A time-dependent global sensitivity framework (52) was used to calculate parametric sensitivity in the two-cell diffusion model. Sensitivity coefficients for a total of 91 system parameters (including parameters of the donor and target cells, as well as TNF- α diffusion) were calculated with respect to the AUC of the nuclear NF- κ B response in the target cell over the 3 hours of lipid A stimulation (of the donor cells). Local sensitivity analysis was performed by simulating single-parameter changes in the two-cell diffusion models, represented as probability of activation (Fig. 5E) or relative change of distance (Fig. 5F). All simulations were performed in MATLAB R2014b. See file S2 for the available codes.

Statistical analysis

All statistical analyses were performed in GraphPad Prism. Data were checked for normality with the D’Agostino-Pearson omnibus test. When normal, parametric tests were performed (standard one-way ANOVA); otherwise, nonparametric Kruskal-Wallis ANOVA was used. Tukey’s or Dunn’s correction for multiple comparisons was applied, respectively.

SUPPLEMENTARY MATERIALS

www.sciencesignaling.org/cgi/content/full/11/540/eaaf3998/DC1
 Fig. S1. NF- κ B reporter cell lines used in the study.
 Fig. S2. FCS calibration of live-cell imaging data.
 Fig. S3. Single-cell NF- κ B p65 responses.
 Fig. S4. Proteomic analysis of TLR4-induced secretion.
 Fig. S5. Temporal analysis of TNF- α production.
 Fig. S6. Larger cells exhibit a stronger *TNFA* response.
 Fig. S7. NF- κ B signaling does not affect the *TNFA* response.
 Fig. S8. Analysis of NF- κ B signaling in primary macrophages.
 Fig. S9. NF- κ B signaling in MEFs does not lead to TNF- α amplification.
 Fig. S10. TNF- α uptake and production across different cell types.
 Fig. S11. IFN- γ enhances TNFR1 abundance in macrophages.
 Fig. S12. Measurements of TNF- α production and loss.
 Fig. S13. Theoretical analysis of TNF- α uptake in small volumes.
 Fig. S14. Proposed model of the NF- κ B signaling pathway in macrophages.
 Fig. S15. Simulated NF- κ B model outputs.
 Fig. S16. Bifurcation analysis of the NF- κ B system.
 Table S1. Summary of TNF- α production measurements.
 Table S2. Single-cell NF- κ B model variables.
 Table S3. Parameterization of the single-cell NF- κ B model.
 Table S4. Parameterization of the two-cell NF- κ B model.
 Movie S1. Untreated RAW264.7 cells.
 Movie S2. Lipid A-stimulated RAW264.7 cells.
 Movie S3. TNF- α -stimulated RAW264.7 cells.
 Movie S4. Lipid A-stimulated BMDMs.
 Movie S5. TNF- α -stimulated BMDMs.
 Model S1. TNF- α half-life in a local tissue environment.
 Model S2. Mathematical model of NF- κ B signaling in macrophages.
 Model S3. Propagation of signaling between producing cells and target cells.
 Model S4. Analysis of autocrine TNF- α feedback.
 File S1. Tabulated smFISH data.
 File S2. Mathematical model files.
 References (69–87)

REFERENCES AND NOTES

1. R. Medzhitov, TLR-mediated innate immune recognition. *Semin. Immunol.* **19**, 1–2 (2007).
2. C. E. Bryant, M. Symmons, N. J. Gay, Toll-like receptor signalling through macromolecular protein complexes. *Mol. Immunol.* **63**, 162–165 (2015).
3. M.-H. Sung, N. Li, Q. Lao, R. A. Gottschalk, G. L. Hager, I. D. C. Fraser, Switching of the relative dominance between feedback mechanisms in lipopolysaccharide-induced NF- κ B signaling. *Sci. Signal.* **7**, ra6 (2014).
4. J. Selimkhanov, B. Taylor, J. Yao, A. Pilko, J. Albeck, A. Hoffmann, L. Tsimring, R. Wollman, Accurate information transmission through dynamic biochemical signaling networks. *Science* **346**, 1370–1373 (2014).
5. Z. Cheng, B. Taylor, D. R. Ourthiague, A. Hoffmann, Distinct single-cell signaling characteristics are conferred by the MyD88 and TRIF pathways during TLR4 activation. *Sci. Signal.* **8**, ra69 (2015).
6. A.-J. Tong, X. Liu, B. J. Thomas, M. M. Lissner, M. R. Baker, M. D. Senagolage, A. L. Allred, G. D. Barish, S. T. Smale, A stringent systems approach uncovers gene-specific mechanisms regulating inflammation. *Cell* **165**, 165–179 (2016).
7. V. R. Ramirez-Carozzi, D. Braas, D. M. Bhatt, C. S. Cheng, C. Hong, K. R. Doty, J. C. Black, A. Hoffmann, M. Carey, S. T. Smale, A unifying model for the selective regulation of inducible transcription by CpG islands and nucleosome remodeling. *Cell* **138**, 114–128 (2009).
8. M. S. Hayden, S. Ghosh, Shared principles in NF- κ B signaling. *Cell* **132**, 344–362 (2008).
9. D. E. Nelson, A. E. C. Ihekweaba, M. Elliott, J. R. Johnson, C. A. Gibney, B. E. Foreman, G. Nelson, V. See, C. A. Horton, D. G. Spiller, S. W. Edwards, H. P. McDowell, J. F. Unitt, E. Sullivan, R. Grimley, N. Benson, D. Broomhead, D. B. Kell, M. R. H. White, Oscillations in NF- κ B signaling control the dynamics of gene expression. *Science* **306**, 704–708 (2004).
10. L. Ashall, C. A. Horton, D. E. Nelson, P. Paszek, C. V. Harper, K. Sillitoe, S. Ryan, D. G. Spiller, J. F. Unitt, D. S. Broomhead, D. B. Kell, D. A. Rand, V. Sée, M. R. H. White, Pulsatile stimulation determines timing and specificity of NF- κ B-dependent transcription. *Science* **324**, 242–246 (2009).
11. P. Paszek, S. Ryan, L. Ashall, K. Sillitoe, C. V. Harper, D. G. Spiller, D. A. Rand, M. R. H. White, Population robustness arising from cellular heterogeneity. *Proc. Natl. Acad. Sci. U.S.A.* **107**, 11644–11649 (2010).
12. J. J. Hughey, M. V. Gutschow, B. T. Bajar, M. W. Covert, Single-cell variation leads to population invariance in NF- κ B signaling dynamics. *Mol. Biol. Cell* **26**, 583–590 (2015).
13. R. A. Kellogg, S. Tay, Noise facilitates transcriptional control under dynamic inputs. *Cell* **160**, 381–392 (2015).
14. S. Tay, J. J. Hughey, T. K. Lee, T. Lipniacki, S. R. Quake, M. W. Covert, Single-cell NF- κ B dynamics reveal digital activation and analogue information processing. *Nature* **466**, 267–271 (2010).
15. S. Hao, D. Baltimore, The stability of mRNA influences the temporal order of the induction of genes encoding inflammatory molecules. *Nat. Immunol.* **10**, 281–288 (2009).
16. J. Pękalski, P. J. Zuk, M. Kocharczyk, M. Junkin, R. Kellogg, S. Tay, T. Lipniacki, Spontaneous NF- κ B activation by autocrine TNF α signaling: A computational analysis. *PLoS ONE* **8**, e78887 (2013).
17. T. K. Lee, E. M. Denny, J. C. Sanghvi, J. E. Gaston, N. D. Maynard, J. J. Hughey, M. W. Covert, A noisy paracrine signal determines the cellular NF- κ B response to lipopolysaccharide. *Sci. Signal.* **2**, ra65 (2009).
18. R. Fischer, R. E. Kontermann, O. Maier, Targeting stNF/TNFR1 signaling as a new therapeutic strategy. *Antibodies* **4**, 48–70 (2015).
19. A. Adamson, C. Boddington, P. Downton, W. Rowe, J. Bagnall, C. Lam, A. Maya-Mendoza, L. Schmidt, C. V. Harper, D. G. Spiller, D. A. Rand, D. A. Jackson, M. R. H. White, P. Paszek, Signal transduction controls heterogeneous NF- κ B dynamics and target gene expression through cytokine-specific refractory states. *Nat. Commun.* **7**, 12057 (2016).
20. A. K. Shalek, R. Satija, J. Shuga, J. J. Trombetta, D. Gennert, D. Lu, P. Chen, R. S. Gertner, J. T. Gaublomme, N. Yosef, S. Schwartz, B. Fowler, J. Wang, X. Wang, R. Ding, R. Raychowdhury, N. Friedman, N. Hacohen, H. Park, A. P. May, A. Regev, Single-cell RNA-seq reveals dynamic paracrine control of cellular variation. *Nature* **510**, 363–369 (2014).
21. Y. Lu, Q. Xue, M. R. Eisele, E. S. Sulistijo, K. Brower, L. Han, E.-a. D. Amir, D. Pe'er, K. Miller-Jensen, R. Fan, Highly multiplexed profiling of single-cell effector functions reveals deep functional heterogeneity in response to pathogenic ligands. *Proc. Natl. Acad. Sci. U.S.A.* **112**, E607–E615 (2015).
22. M. Junkin, A. J. Kaestli, Z. Cheng, C. Jordi, C. Albayrak, A. Hoffmann, S. Tay, High-content quantification of single-cell immune dynamics. *Cell Rep.* **15**, 411–422 (2016).
23. K. E. Tkach, D. Barik, G. Voisinne, N. Malandro, M. M. Hathorn, J. W. Cotari, R. Vogel, T. Merghoub, J. Wolchok, O. Krichevsky, G. Altan-Bonnet, T cells translate individual, quantal activation into collective, analog cytokine responses via time-integrated feedbacks. *eLife* **3**, e01944 (2014).
24. H. Youk, W. A. Lim, Sending mixed messages for cell population control. *Cell* **158**, 973–975 (2014).
25. J. Bauer, F. A. Bahmer, J. Wörl, W. Neuhuber, G. Schuler, M. Fartasch, A strikingly constant ratio exists between Langerhans cells and other epidermal cells in human skin. A stereologic study using the optical disector method and the confocal laser scanning microscope. *J. Invest. Dermatol.* **116**, 313–318 (2001).
26. S. Epelman, K. J. Lavine, G. J. Randolph, Origin and functions of tissue macrophages. *Immunity* **41**, 21–35 (2014).
27. X. Zhou, R. A. Franklin, M. Adler, J. B. Jacox, W. Bailis, J. A. Shyer, R. A. Flavell, A. E. Mayo, U. Alon, R. Medzhitov, Circuit design features of a stable two-cell system. *Cell* **172**, 744–757.e17 (2018).
28. J. Kezic, H. Xu, H. R. Chinnery, C. C. Murphy, P. G. McMenamin, Retinal microglia and uveal tract dendritic cells and macrophages are not CX3CR1 dependent in their recruitment and distribution in the young mouse eye. *Invest. Ophthalmol. Vis. Sci.* **49**, 1599–1608 (2008).
29. R. Yamasaki, H. Lu, O. Butovsky, N. Ohno, A. M. Rietsch, R. Cialic, P. M. Wu, C. E. Doykan, J. Lin, A. C. Coteleur, G. Kidd, M. M. Zorlu, N. Sun, W. Hu, L. Liu, J.-C. Lee, S. E. Taylor, L. Uehlein, D. Dixon, J. Gu, C. M. Floruta, M. Zhu, I. F. Charo, H. L. Weiner, R. M. Ransohoff, Differential roles of microglia and monocytes in the inflamed central nervous system. *J. Exp. Med.* **211**, 1533–1549 (2014).
30. L. Beattie, M. d'El-Rei Hermida, J. W. J. Moore, A. Maroof, N. Brown, D. Lagos, P. M. Kaye, A transcriptomic network identified in uninfected macrophages responding to inflammation controls intracellular pathogen survival. *Cell Host Microbe* **14**, 357–368 (2013).
31. L. Chorro, A. Sarde, M. Li, K. J. Woollard, P. Chambon, B. Malissen, A. Kissenpfennig, J.-B. Barbaroux, R. Groves, F. Geissmann, Langerhans cell (LC) proliferation mediates neonatal development, homeostasis, and inflammation-associated expansion of the epidermal LC network. *J. Exp. Med.* **206**, 3089–3100 (2009).
32. P. Yde, B. Mengel, M. H. Jensen, S. Krishna, A. Trusina, Modeling the NF- κ B mediated inflammatory response predicts cytokine waves in tissue. *BMC Syst. Biol.* **5**, 115 (2011).
33. A. J. Muller, O. Filipe-Santos, G. Eberl, T. Aebischer, G. F. Späth, P. Bousso, CD4+ T cells rely on a cytokine gradient to control intracellular pathogens beyond sites of antigen presentation. *Immunity* **37**, 147–157 (2012).
34. D. Busse, M. de la Rosa, K. Hobiger, K. Thurley, M. Flossdorf, A. Scheffold, T. Höfer, Competing feedback loops shape IL-2 signaling between helper and regulatory T lymphocytes in cellular microenvironments. *Proc. Natl. Acad. Sci. U.S.A.* **107**, 3058–3063 (2010).
35. K. Thurley, D. Gerecht, E. Friedmann, T. Hofer, Three-dimensional gradients of cytokine signaling between T cells. *PLoS Comput. Biol.* **11**, e1004206 (2015).
36. K. Francis, B. O. Palsson, Effective intercellular communication distances are determined by the relative time constants for cyto/chemokine secretion and diffusion. *Proc. Natl. Acad. Sci. U.S.A.* **94**, 12258–12262 (1997).
37. A. Oyler-Yaniv, J. Oyler-Yaniv, B. M. Whitlock, Z. Liu, R. N. Germain, M. Huse, G. Altan-Bonnet, O. Krichevsky, A tunable diffusion-consumption mechanism of cytokine propagation enables plasticity in cell-to-cell communication in the immune system. *Immunity* **46**, 609–620 (2017).
38. J. Bagnall, C. Boddington, J. Boyd, R. Brignall, W. Rowe, N. A. Jones, L. Schmidt, D. G. Spiller, M. R. H. White, P. Paszek, Quantitative dynamic imaging of immune cell signalling using lentiviral gene transfer. *Integr. Biol.* **7**, 713–725 (2015).
39. C. R. Raetz, C. M. Reynolds, M. S. Trent, R. E. Bishop, Lipid A modification systems in gram-negative bacteria. *Annu. Rev. Biochem.* **76**, 295–329 (2007).
40. F. Mueller, A. Senecal, K. Tantale, H. Marie-Nelly, N. Ly, O. Collin, E. Basyuk, E. Bertrand, X. Darzacq, C. Zimmer, FISH-quant: Automatic counting of transcripts in 3D FISH images. *Nat. Methods* **10**, 277–278 (2013).
41. M. B. Elowitz, A. J. Levine, E. D. Siggia, P. S. Swain, Stochastic gene expression in a single cell. *Science* **297**, 1183–1186 (2002).
42. A. Rhee, R. Cheong, A. Levchenko, Noise decomposition of intracellular biochemical signaling networks using nonequivalent reporters. *Proc. Natl. Acad. Sci. U.S.A.* **111**, 17330–17335 (2014).
43. O. Padovan-Merhar, G. P. Nair, A. G. Bialesch, A. Mayer, S. Scarfone, S. W. Foley, A. R. Wu, L. S. Churchman, A. Singh, A. Raj, Single mammalian cells compensate for differences in cellular volume and DNA copy number through independent global transcriptional mechanisms. *Mol. Cell* **58**, 339–352 (2015).
44. S. Zhang, C. C. Kim, S. Batra, J. H. McKerrow, P. Loke, Delineation of diverse macrophage activation programs in response to intracellular parasites and cytokines. *PLoS Negl. Trop. Dis.* **4**, e648 (2010).
45. T. Frank, S. Tay, Automated co-culture system for spatiotemporal analysis of cell-to-cell communication. *Lab Chip* **15**, 2192–2200 (2015).
46. A. Sica, A. Mantovani, Macrophage plasticity and polarization: In vivo veritas. *J. Clin. Invest.* **122**, 787–795 (2012).

47. Q. Xue, Y. Lu, M. R. Eisele, E. S. Sulistijo, N. Khan, R. Fan, K. Miller-Jensen, Analysis of single-cell cytokine secretion reveals a role for paracrine signaling in coordinating macrophage responses to TLR4 stimulation. *Sci. Signal.* **8**, ra59 (2015).
48. A. Hoffmann, A. Levchenko, M. L. Scott, D. Baltimore, The I κ B-NF- κ B signaling module: Temporal control and selective gene activation. *Science* **298**, 1241–1245 (2002).
49. J. R. Bradley, D. R. Johnson, J. S. Pober, Four different classes of inhibitors of receptor-mediated endocytosis decrease tumor necrosis factor-induced gene expression in human endothelial cells. *J. Immunol.* **150**, 5544–5555 (1993).
50. M. Tsujimoto, Y. K. Yip, J. Vilcek, Tumor necrosis factor: Specific binding and internalization in sensitive and resistant cells. *Proc. Natl. Acad. Sci. U.S.A.* **82**, 7626–7630 (1985).
51. N. Watanabe, H. Kuriyama, H. Sone, H. Neda, N. Yamauchi, M. Maeda, Y. Niitsu, Continuous internalization of tumor necrosis factor receptors in a human myosarcoma cell line. *J. Biol. Chem.* **263**, 10262–10266 (1988).
52. B. P. Ingalls, H. M. Sauro, Sensitivity analysis of stoichiometric networks: An extension of metabolic control analysis to non-steady state trajectories. *J. Theor. Biol.* **222**, 23–36 (2003).
53. R. A. Gottschalk, A. J. Martins, B. R. Angermann, B. Dutta, C. E. Ng, S. Uderhardt, J. S. Tsang, I. D. Fraser, M. Meier-Schellersheim, R. N. Germain, Distinct NF- κ B and MAPK activation thresholds uncouple steady-state microbe sensing from anti-pathogen inflammatory responses. *Cell Syst.* **2**, 378–390 (2016).
54. S. J. Jenkins, D. A. Hume, Homeostasis in the mononuclear phagocyte system. *Trends Immunol.* **35**, 358–367 (2014).
55. J. M. Ankers, R. Awais, N. A. Jones, J. Boyd, S. Ryan, A. D. Adamson, C. V. Harper, L. Bridge, D. G. Spiller, D. A. Jackson, P. Paszek, V. Sée, M. R. White, Dynamic NF- κ B and E2F interactions control the priority and timing of inflammatory signalling and cell proliferation. *eLife* **5**, e10473 (2016).
56. R. E. Lee, S. R. Walker, K. Savery, D. A. Frank, S. Gaudet, Fold change of nuclear NF- κ B determines TNF-induced transcription in single cells. *Mol. Cell* **53**, 867–879 (2014).
57. Q. Li, B. J. Cherayil, Role of toll-like receptor 4 in macrophage activation and tolerance during *Salmonella enterica* serovar typhimurium infection. *Infect. Immun.* **71**, 4873–4882 (2003).
58. J. G. Cannon, R. G. Tompkins, J. A. Gelfand, H. R. Michie, G. G. Stanford, J. W. van der Meer, S. Endres, G. Lonnemann, J. Corsetti, B. Chernow, D. W. Wilmore, S. M. Wolff, J. F. Burke, C. A. Dinarello, Circulating interleukin-1 and tumor necrosis factor in septic shock and experimental endotoxin fever. *J. Infect. Dis.* **161**, 79–84 (1990).
59. S. Xanthoulea, M. Pasparakis, S. Kousteni, C. Brakebusch, D. Wallach, J. Bauer, H. Lassmann, G. Kollias, Tumor necrosis factor (TNF) receptor shedding controls thresholds of innate immune activation that balance opposing TNF functions in infectious and inflammatory diseases. *J. Exp. Med.* **200**, 367–376 (2004).
60. A. B. Caldwell, Z. Cheng, J. D. Vargas, H. A. Birnbaum, A. Hoffmann, Network dynamics determine the autocrine and paracrine signaling functions of TNF. *Genes Dev.* **28**, 2120–2133 (2014).
61. R. Brignall, P. Cauchy, S. L. Bevington, B. Gorman, A. O. Pisco, J. Bagnall, C. Boddington, W. Rowe, H. England, K. Rich, L. Schmidt, N. P. Dyer, M. A. Travis, S. Ott, D. A. Jackson, P. N. Cockerill, P. Paszek, Integration of kinase and calcium signaling at the level of chromatin underlies inducible gene activation in T cells. *J. Immunol.* **199**, 2652–2667 (2017).
62. S. Gong, X. W. Yang, Modification of bacterial artificial chromosomes (BACs) and preparation of intact BAC DNA for generation of transgenic mice. *Curr. Protoc. Neurosci. Chapter 5*, Unit 5.21 (2005).
63. G. Rabut, J. Ellenberg, Automatic real-time three-dimensional cell tracking by fluorescence microscopy. *J. Microsc.* **216**, 131–137 (2004).
64. H. Shen, G. Nelson, D. E. Nelson, S. Kennedy, D. G. Spiller, T. Griffiths, N. Paton, S. G. Oliver, M. R. White, D. B. Kell, Automated tracking of gene expression in individual cells and cell compartments. *J. R. Soc. Interface* **3**, 787–794 (2006).
65. J. R. Wisniewski, A. Zougman, N. Nagaraj, M. Mann, Universal sample preparation method for proteome analysis. *Nat. Methods* **6**, 359–362 (2009).
66. J. Zhang, W. Yang, S. Li, S. Yao, P. Qi, Z. Yang, Z. Feng, J. Hou, L. Cai, M. Yang, W. Wu, D.-a. Guo, An intelligentized strategy for endogenous small molecules characterization and quality evaluation of earthworm from two geographic origins by ultra-high performance HILIC/QTOF MS^E and Progenesis Q1. *Anal. Bioanal. Chem.* **408**, 3881–3890 (2016).
67. J. A. Vizcaino, E. W. Deutsch, R. Wang, A. Csordas, F. Reisinger, D. Rios, J. A. Dienes, Z. Sun, T. Farrar, N. Bandeira, P. A. Binz, I. Xenarios, M. Eisenacher, G. Mayer, L. Gatto, A. Campos, R. J. Chalkley, H.-J. Kraus, J. P. Albar, S. Martinez-Bartolomé, R. Apweiler, G. S. Omenn, L. Martens, A. R. Jones, H. Hermjakob, ProteomeXchange provides globally coordinated proteomics data submission and dissemination. *Nat. Biotechnol.* **32**, 223–226 (2014).
68. D. Waggott, K. Chu, S. Yin, B. G. Wouters, F. F. Liu, P. C. Boutros, NanoStringNorm: An extendable R package for the pre-processing of NanoString mRNA and miRNA data. *Bioinformatics* **28**, 1546–1548 (2012).
69. T. Mijatovic, L. Houzet, P. Defrance, L. Droogmans, G. Huez, V. Krums, Tumor necrosis factor- α mRNA remains unstable and hypoadenylated upon stimulation of macrophages by lipopolysaccharides. *Eur. J. Biochem.* **267**, 6004–6012 (2000).
70. F. Carlotti, S. K. Dower, E. E. Qvarnstrom, Dynamic shuttling of nuclear factor κ B between the nucleus and cytoplasm as a consequence of inhibitor dissociation. *J. Biol. Chem.* **275**, 41028–41034 (2000).
71. K. Imamura, D. Spriggs, D. Kufe, Expression of tumor necrosis factor receptors on human monocytes and internalization of receptor bound ligand. *J. Immunol.* **139**, 2989–2992 (1987).
72. A. Pradinesfigueres, C. R. Raetz, Processing and secretion of tumor-necrosis-factor-alpha in endotoxin-treated mono mac-6 cells are dependent on phorbol-myristate acetate. *J. Biol. Chem.* **267**, 23261–23268 (1992).
73. E. G. Lee, D. L. Boone, S. Chai, S. L. Libby, M. Chien, J. P. Lodolce, A. Ma, Failure to regulate TNF-induced NF- κ B and cell death responses in A20-deficient mice. *Science* **289**, 2350–2354 (2000).
74. M. Matmati, P. Jacques, J. Maelfait, E. Verheugen, M. Kool, M. Sze, L. Geboes, E. Louagie, C. Mc Guire, L. Vereecke, Y. Y. Chu, L. Boon, S. Staelens, P. Matthys, B. N. Lambrecht, M. Schmidt-Suppran, M. Pasparakis, D. Elewaut, R. Beyaert, G. van Loo, A20 (TNFAIP3) deficiency in myeloid cells triggers erosive polyarthritis resembling rheumatoid arthritis. *Nat. Genet.* **43**, 908–129 (2011).
75. L. Vande Walle, N. Van Opendenbosch, P. Jacques, A. Fossoul, E. Verheugen, P. Vogel, R. Beyaert, D. Elewaut, T.-D. Kanneganti, G. van Loo, M. Lamkanfi, Negative regulation of the NLRP3 inflammasome by A20 protects against arthritis. *Nature* **512**, 69–73 (2014).
76. S. Schutze, V. Tchikov, W. Schneider-Brachert, Regulation of TNFR1 and CD95 signalling by receptor compartmentalization. *Nat. Rev. Mol. Cell Biol.* **9**, 655–662 (2008).
77. T. Lipniacki, K. Puszynski, P. Paszek, A. R. Brasier, M. Kimmel, Single TNF α trimers mediating NF- κ B activation: Stochastic robustness of NF- κ B signaling. *BMC Bioinformatics* **8**, 376 (2007).
78. A. Hoffmann, D. Baltimore, Circuitry of nuclear factor κ B signaling. *Immunol. Rev.* **210**, 171–186 (2006).
79. S. K. Biswas, E. Lopez-Collazo, Endotoxin tolerance: New mechanisms, molecules and clinical significance. *Trends Immunol.* **30**, 475–487 (2009).
80. M. Delhase, M. Hayakawa, Y. Chen, M. Karin, Positive and negative regulation of I κ B kinase activity through IKK β subunit phosphorylation. *Science* **284**, 309–313 (1999).
81. K. Enesa, M. Zakkari, H. Chaudhury, L. A. Luong, L. Rawlinson, J. C. Mason, D. O. Haskard, J. L. E. Dean, P. C. Evans, NF- κ B suppression by the deubiquitinating enzyme Cezanne—A novel negative feedback loop in pro-inflammatory signaling. *J. Biol. Chem.* **283**, 7036–7045 (2008).
82. K. Verhelst, I. Carpentier, M. Kreike, L. Meloni, L. Verstrepen, T. Kenschke, I. Dikic, R. Beyaert, A20 inhibits LUBAC-mediated NF- κ B activation by binding linear polyubiquitin chains via its zinc finger 7. *EMBO J.* **31**, 3845–3855 (2012).
83. H.-T. Yang, S. Papoutsopoulou, M. Belich, C. Brender, J. Janzen, T. Gantke, M. Handley, S. C. Ley, Coordinate regulation of TPL-2 and NF- κ B signaling in macrophages by NF- κ B1 p105. *Mol. Cell Biol.* **32**, 3438–3451 (2012).
84. H. Fujita, S. Rahighi, M. Akita, R. Kato, Y. Sasaki, S. Wakatsuki, K. Iwai, Mechanism underlying I κ B kinase activation mediated by the linear ubiquitin chain assembly complex. *Mol. Cell Biol.* **34**, 1322–1335 (2014).
85. K. Oda, H. Kitano, A comprehensive map of the toll-like receptor signaling network. *Mol. Syst. Biol.* **2**, 2006.0015 (2006).
86. T. Lipniacki, P. Paszek, A. R. Brasier, B. Luxon, M. Kimmel, Mathematical model of NF- κ B regulatory module. *J. Theor. Biol.* **228**, 195–215 (2004).
87. Y. J. Wang, P. Paszek, C. A. Horton, H. Yue, M. R. H. White, D. B. Kell, M. R. Muldoon, D. S. Broomhead, A systematic survey of the response of a model NF- κ B signalling pathway to TNF alpha stimulation. *J. Theor. Biol.* **297**, 137–147 (2012).

Acknowledgments: We thank members of the Systems Microscopy Centre and K. Couper for discussion and S. Lyst, S. Papoutsopoulou, and E. Borysiewicz in Manchester and R. Naumann and the Max Planck Institute of Molecular Cell Biology, Dresden, Germany, for the development of transgenic animals. We also thank P. J. Foster for assessing all of the statistical analyses for this study. **Funding:** P.P. was supported by a UK Biotechnology and Biological Sciences Research Council (BBSRC) David Phillips Research Fellowship (BB/1017976/1). This work was also supported by Medical Research Council (UK) (MR/K015885/1), BBSRC (BB/K003097/1 and BB/R007691/1), and the Wellcome Trust (097820/Z/11/B). The work was funded by the European Union Seventh Framework Programme (FP7/2012-2017) under grant agreement no. 305564. **Author contributions:** J. Bagnall developed the study; constructed stable cells; performed time-lapse imaging, smFISH, and ELISA experiments; and analyzed the data. C.B. developed mathematical modeling, performed TNF- α internalization experiments, and analyzed the data. H.E. performed primary cell imaging experiments. R.B. assisted with ELISA assays. P.D., supervised by M.R.H.W., performed PCR analyses and assisted with smFISH development. J. Boyd, supervised by M.R.H.W., performed FCS analyses. W.R. analyzed genomics data. Z.A. and A.B. analyzed mathematical models. N.M.X.P. assisted with smFISH

experiments. R.O. performed secretome analysis. L.S. assisted with cell line development. A.A. and C.W., under the supervision of M.R.H.W., D.A.J., and W.M., developed BAC constructs and transgenic animals. D.G.S. and M.R.H.W. supported imaging analyses. M.M. supervised Z.A. and assisted with modeling analyses. P.P. wrote the manuscript with the assistance of J. Bagnall, C.B., D.G.S., M.R.H.W., and M.M. P.P. directed the study. **Competing interests:** The authors declare that they have no competing interests. **Data and materials availability:** All data are available from the authors upon request. Lentiviral constructs and developed cell lines require material transfer agreements. The proteomics data are deposited with the ProteomeXchange Consortium through the PRIDE repository with the data set identifier PXD001905 and 10.6019/PXD001905. All other data needed to evaluate the conclusions in the paper are present in the paper or the Supplementary Materials.

Submitted 5 February 2016

Accepted 3 July 2018

Published 24 July 2018

10.1126/scisignal.aaf3998

Citation: J. Bagnall, C. Boddington, H. England, R. Brignall, P. Downton, Z. Alsoufi, J. Boyd, W. Rowe, A. Bennett, C. Walker, A. Adamson, N. M. X. Patel, R. O’Cualain, L. Schmidt, D. G. Spiller, D. A. Jackson, W. Müller, M. Muldoon, M. R. H. White, P. Paszek, Quantitative analysis of competitive cytokine signaling predicts tissue thresholds for the propagation of macrophage activation. *Sci. Signal.* **11**, eaaf3998 (2018).

Quantitative analysis of competitive cytokine signaling predicts tissue thresholds for the propagation of macrophage activation

James Bagnall, Christopher Boddington, Hazel England, Ruth Brignall, Polly Downton, Zainab Alsoufi, James Boyd, William Rowe, Alexander Bennett, Catherine Walker, Antony Adamson, Nisha M. X. Patel, Ronan O'Cualain, Lorraine Schmidt, David G. Spiller, Dean A. Jackson, Werner Müller, Mark Muldoon, Michael R. H. White and Pawel Paszek

Sci. Signal. **11** (540), eaaf3998.
DOI: 10.1126/scisignal.aaf3998

Modeling TNF- α signaling by macrophages

The proinflammatory cytokine TNF- α is one of the earliest factors secreted by macrophages in response to bacterial infection. Diffusion of TNF- α throughout tissues disseminates the inflammatory response; however, without mechanisms to limit TNF- α signaling, damaging chronic inflammation would occur. Through single-cell monitoring of the dynamics of gene expression in macrophages and of TNF- α secretion and uptake by macrophages and fibroblasts, Bagnall *et al.* derived a mathematical model that suggests that TNF- α secreted by macrophages in tissues acts locally to drive immune responses but that it is taken up by surrounding nonimmune cells, such as fibroblasts, to limit its long-range effects in the tissue.

| | |
|-------------------------|--|
| ARTICLE TOOLS | http://stke.sciencemag.org/content/11/540/eaaf3998 |
| SUPPLEMENTARY MATERIALS | http://stke.sciencemag.org/content/suppl/2018/07/20/11.540.eaaf3998.DC1 |
| RELATED CONTENT | http://stke.sciencemag.org/content/sigtrans/11/518/eaal2434.full http://stke.sciencemag.org/content/sigtrans/11/511/eaan0790.full http://stke.sciencemag.org/content/sigtrans/11/511/eaao4910.full http://science.sciencemag.org/content/sci/354/6315/999.full http://stm.sciencemag.org/content/scitransmed/9/421/eaag3214.full http://stm.sciencemag.org/content/scitransmed/10/430/eaao2731.full |
| REFERENCES | This article cites 87 articles, 37 of which you can access for free http://stke.sciencemag.org/content/11/540/eaaf3998#BIBL |
| PERMISSIONS | http://www.sciencemag.org/help/reprints-and-permissions |

Use of this article is subject to the [Terms of Service](#)